



**Budapest University of Technology and Economics**

Faculty of Electrical Engineering and Informatics

Department of Control Engineering and Information Technology



**Institute for Computer Science and Control**

Systems and Control Laboratory

# **Visual-inertial navigation with intermittent or spoofed GPS information**

SCIENTIFIC STUDENTS' ASSOCIATION REPORT

*Author*

Zsombor Novozánszki

*Advisor*

Dr. Emese Szádeczky-Kardoss Gincsiné

Dr. Péter Bauer

November 2, 2023

# CONTENTS

---

<b>Kivonat</b>	<b>iv</b>
<b>Abstract</b>	<b>vi</b>
<b>1 Introduction</b>	<b>1</b>
1.1 Structure of the paper . . . . .	3
<b>2 Mathematical foundations</b>	<b>5</b>
2.1 Navigation frames . . . . .	6
2.1.1 North-East-Down reference frame . . . . .	6
2.1.2 Body frame . . . . .	7
2.2 Camera frames . . . . .	9
2.2.1 Camera system . . . . .	9
2.2.2 Pinhole camera projection . . . . .	10
2.3 Quaternions . . . . .	11
<b>3 Introduction of the applied filter technique</b>	<b>14</b>
3.1 Error-state kinematics . . . . .	15
3.1.1 Kalman filter states for IMU driven systems . . . . .	15
3.1.2 ESKF states . . . . .	16
3.1.3 Error-state kinematics in discrete time . . . . .	19
3.2 Measurement equation . . . . .	21
3.3 ESKF framework . . . . .	21

3.3.1	Prediction step . . . . .	22
3.3.2	Update step . . . . .	23
3.3.3	Error injection into the nominal-state . . . . .	25
<b>4</b>	<b>Overview of the triangulation method</b>	<b>27</b>
4.1	Problem statement . . . . .	27
4.1.1	Line of sight (LOS) measurements . . . . .	29
4.2	LOST method . . . . .	29
4.2.1	Covariance calculations . . . . .	30
4.2.2	The optimal solution . . . . .	31
4.2.3	Practical formalization of the estimator . . . . .	32
4.2.4	Covariance of the estimator . . . . .	32
4.3	The recursive version . . . . .	33
<b>5</b>	<b>Synergizing LOST and ESKF for robust navigation</b>	<b>34</b>
5.1	The modified Kalman gain . . . . .	34
5.2	Cross-covariance estimation . . . . .	36
<b>6</b>	<b>Development</b>	<b>38</b>
6.1	Camera configuration . . . . .	38
6.2	Simulation setup . . . . .	39
<b>7</b>	<b>Conclusion</b>	<b>45</b>
<b>A</b>	<b>Quaternion operations</b>	<b>46</b>
A.1	Rotation vector to quaternion formula . . . . .	47
A.2	The time derivative of quaternion . . . . .	47
A.3	Jacobian of quaternion rotation with respect to the vector . . . . .	49

A.4	Jacobian of quaternion rotation with respect to the quaternion . . .	49
<b>B</b>	<b>ESKF-related equations</b>	<b>50</b>
B.1	True rotation matrix . . . . .	50
B.2	Error-state equations . . . . .	51
B.2.1	Position error . . . . .	51
B.2.2	Angular error . . . . .	52
B.2.3	Velocity error . . . . .	53
B.3	Jacobian of true quaternion with respect to the error rotation vector	54
B.4	Jacobian of reset function ( $g$ ) with respect to the error rotation vector	54
	<b>Abbreviations</b>	<b>56</b>
	<b>List of Figures</b>	<b>57</b>
	<b>List of Tables</b>	<b>57</b>
	<b>Bibliography</b>	<b>58</b>

# KIVONAT

---

Az elmúlt évtizedekben a pilóta nélküli légi járművek (Unmanned Aerial Vehicle, UAV) egyre népszerűbbé váltak civil és akadémiai alkalmazásokban is, mint például felderítés, áruszállítás, geofizikai adatgyűjtés, mentési műveletek vagy éppen mezőgazdasági célú felhasználás. Az előrelépés nemcsak a technikai modernizációnak köszönhető, hanem a szélesebb körű felhasználhatóságnak, ami nagyban a hagyományos navigációs módszerek innovációjának köszönhető. A UAV-k jövőre gyakorolt hatása azon is múlik mennyire tudnak jól navigálni GPS (Global Positioning System) nélküli környezetben például kimaradó, zavart (jamming) vagy hamisított (spoofing) jelek esetén.

Dolgozatom középpontjában egy vizuális-inerciális navigációs algoritmus áll. A tanulmány során megvalósított rendszer célja meghatározni egy légi jármű pozícióját, orientációját, sebességét és a gyorsulás és szögsebesség szenzor bias értékeit inerciális szenzorrendszer (Inertial Measurement Unit, IMU) mérések és mono kameraképek alapján. A javasolt rendszer egy hiba állapot Kálmán-szűrő (Error-State Kalman Filter, ESKF) alapú keretrendszerben hajtja végre az IMU és a kamera adatok integrációját. Az IMU mérésekből a repülőgép pozícióját, sebességét és orientációját lehet becsülni, amelynek hibáját a kamera képekből nyert információval korrigálom. A korrekció során felhasznált jellegpontok pozícióját háromszögelés útján számítom, amelyhez egy ún. LOST (Linear Optimal Sine Triangulation) módszert alkalmazok. Az algoritmus tesztelése úgy történik, hogy a kezdeti állapotban ismert GPS koordinátákat feltételezek, és ez idő alatt már megkezdődik a jellegpontok pozíciójának optimalizációja, amelyeket az ESKF frissítési fázisában használok fel. Később a GPS koordináták már nem ismertek, ezért az ESKF becslésekből történik az újabb jellegpontok pozíciójának optimalizációja, azok alapján pedig a frissítés. Munkámban megvizsgálom a módszer pontosságának korlátait, és azt is, hogy a GPS jel elvesztése után meddig ad kielégítő pontosságot csak a vizuális-inerciális navigáció.

Összefoglalva, a dolgozat bemutatja az algoritmus fejlesztését, amely fuzionálja az inerciális és vizuális adatokat, valamint az ehhez szükséges elméleti alapismereteket és matematikai módszertanokat. Az alap algoritmusokat (ESKF és LOST) szakirodalomból vettem, amelyeket saját rendszerbe integráltam. A kutatás során először egy szimulációt hoztam létre, amelyet fokozatosan közelítettem a valóságos körülményeket leginkább modellező környezethez. Az ígéretes szimulációs eredményeket követően fő célom az elkészített navigációs rendszer tesztelése lesz szintetikus vagy valós felvételeken.

# ABSTRACT

---

Over the past decades, Unmanned Aerial Vehicles (UAVs) have become increasingly popular in both civilian and academic applications, such as exploration, cargo delivery, geophysical data collection, rescue operations, and agricultural purposes. This expansion required not only technical modernization but also advancement in traditional navigation methods. The future impact of UAVs also depends on their ability to navigate effectively in GPS (Global Positioning System)-denied environments, for example, scenarios involving signal dropout, jamming, or spoofing.

My work focuses on a visual-inertial navigation algorithm. In this study, the implemented system's goal is to determine an aircraft's position, orientation, velocity, and bias values of the accelerometer and gyroscope based on measurements from an Inertial Measurement Unit (IMU) and monocular camera images. The proposed system performs the integration of IMU and camera data within an Error-State Kalman Filter (ESKF) framework. The aircraft's position, velocity, and orientation are estimated from IMU measurements, and these estimates are corrected with the information obtained from camera images. During the correction, the positions of feature points are computed through triangulation using a method called Linear Optimal Sine Triangulation (LOST). The algorithm is tested as follows: in the initial stage the GPS coordinates are assumed to be known, and the optimization of feature point positions begins this time, and they are utilized in the ESKF update. Later, when GPS coordinates are no longer known, the optimization of feature point positions is based on the ESKF estimates, and these optimized values are used in the update. In my work, I examine the limitations of the method's accuracy and investigate how long it can provide satisfactory accuracy after losing the GPS signal, relying only on visual-inertial navigation.

To summarize, the thesis presents the development of an algorithm that fuses inertial and visual data besides the required theoretical background and mathematical foundations. The utilized algorithms (ESKF and LOST) were chosen from the literature and integrated into the newly developed system. I applied a simulation environment and a gradual approach during the development process, starting with ideal conditions and incrementally introducing more realistic elements to the simulation. After achieving promising simulation results, my primary objective in the future is to test the developed navigation system on synthetic or real-world footage.



# CHAPTER 1

## INTRODUCTION

---

Until the early 2000s Unmanned Aerial Vehicles (UAV) have been limited to the defense and military industries, because of the high costs and the complexity of constructing these vehicles. Nevertheless, they have become cheaper and more available in several civil and academic applications over the past decades. They have not just turned more common, but their capabilities have dramatically increased, therefore they are more popular and widely used in applications such as rescue operations [1], data collection and geophysics exploration [2], inspections [3], and agricultural purposes [4].

This expansion required not only technical developments but advancement in traditional navigation methods, where Global Positioning System (GPS) is combined with Inertial Navigation System (INS), creating GPS-INS system [5]. The small unmanned aircraft's future impact depends on how well they can navigate in GPS-denied environments such as narrow city corridors or circumstances with GPS disturbance or spoofing. Inertial measurements by themselves can be used to estimate the position of the aircraft respected to a known initial position, but they will accumulate errors over time, especially with low-cost Inertial Measurement Unit (IMU) sensors. This phenomenon is usually called drift because estimated values drift away from the true values with time.

In order to give a better estimation of the position in most GPS-free applications exteroceptive sensors are used such as cameras, laser scanners, distance sensors, etc.. The type of used sensor mostly depends on the kind of vehicle. For example only considering UAVs, a multicopter drone has completely different aircraft dynamics, mission profile, and sensing requirements compared to fixed-wing aircraft. Since fixed-wing aircraft usually fly at high altitudes above the environ-

ment with relatively high speeds, distance sensors are ineffective. In this case, the most common approach is using cameras for instance, both [6] and [7] leverage visual information captured by cameras and integrate this data with measurements from an IMU to estimate the motion of the aircraft. When an algorithm fails to close the navigation loop, particularly in the absence of external absolute positioning references like GPS, it results in the estimates drift, which emerges due to the algorithm's inability to establish consistent and accurate reference points or constraints, thereby leading to unbounded cumulative errors over time.

The measurement fusion and sensor noise filtering can take place in an Extended Kalman Filter (EKF) framework because typically these are nonlinear systems. EKFs can be used on any kind of vehicle including robots [8], Unmanned Aerial Systems(UAS) [9, 10], etc. They can account for both sensor errors and process uncertainty, but it is important to note that these methods only work well when errors remain small, e.g. when the availability of GPS measurements makes it possible to regularly remove drift errors. When GPS or any other global measurements are unavailable for a longer period of time, the global position and yaw angle of the aircraft is unobservable, which eventually leads to the divergence of estimates [11, 12]. In addition, if an EKF receives a global measurement after significant drift errors have accumulated, nonlinearities can complicate the utilization of the measurement, and it could result in large jumps in the estimate, in some cases it can even lead to filter divergence. This is because the local linearization of the measurement equations around the drifted states is applied, which can present incorrect dynamics.

In recent years a new method was proposed called relative navigation [13, 14], which is able to handle these observability and consistency problems. With exteroceptive sensors we are able to navigate with respect to the surroundings, hence this method can be divided into a relative front-end and a global back-end, the complete architecture is shown in Figure 1.1. The front end provides an estimation of the state relative to the local environment, while the back end is basically an optimization algorithm, which uses the calculations of the front end to produce global estimates. Several important observability and computational bene-

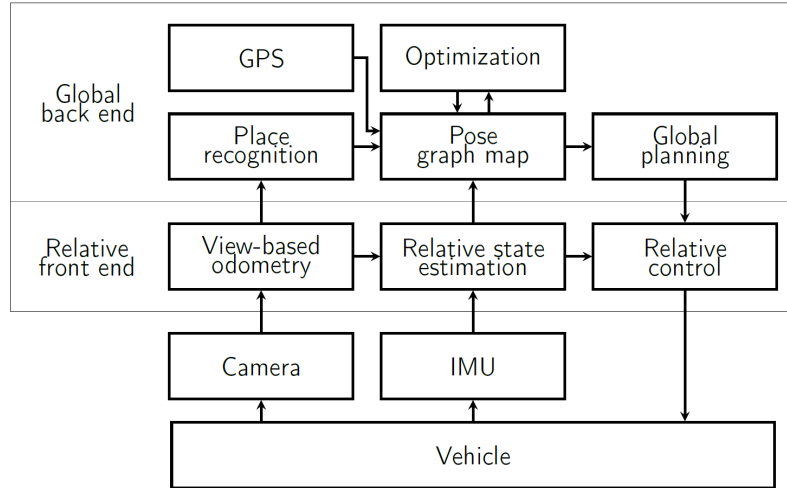


**Figure 1.1:** Block diagram of relative navigation ([7]: page 2, Figure 2)

fits are obtained by dividing the architecture into a relative front end and a global back end:

- The front end calculates the estimate relative to a local frame, where the states can remain observable and the uncertainty can be accurately represented by a Gaussian distribution. This enables the utilization of the computational advantage of an Error-State Kalman Filter (ESKF), which is a better solution, than an ordinary EKF because it calculates the nominal state according to the original non-linear dynamics, therefore the linearization around this state is a better approximation.
- On the other hand, the back end uses a graph that can effectively represent nonlinearities in heading and can be robustly optimized with additional constraints, such as opportunistic global measurements or place recognition.

In this paper, a visual-inertial navigation algorithm will be presented, which is based on [7]. The target UAV is a fixed-wing aircraft called Sindy, shown in Figure 1.2.

## 1.1 Structure of the paper

To sum up the involved steps during the project, the primary objective was to integrate a visual-inertial ESKF into a simulation that was already available to

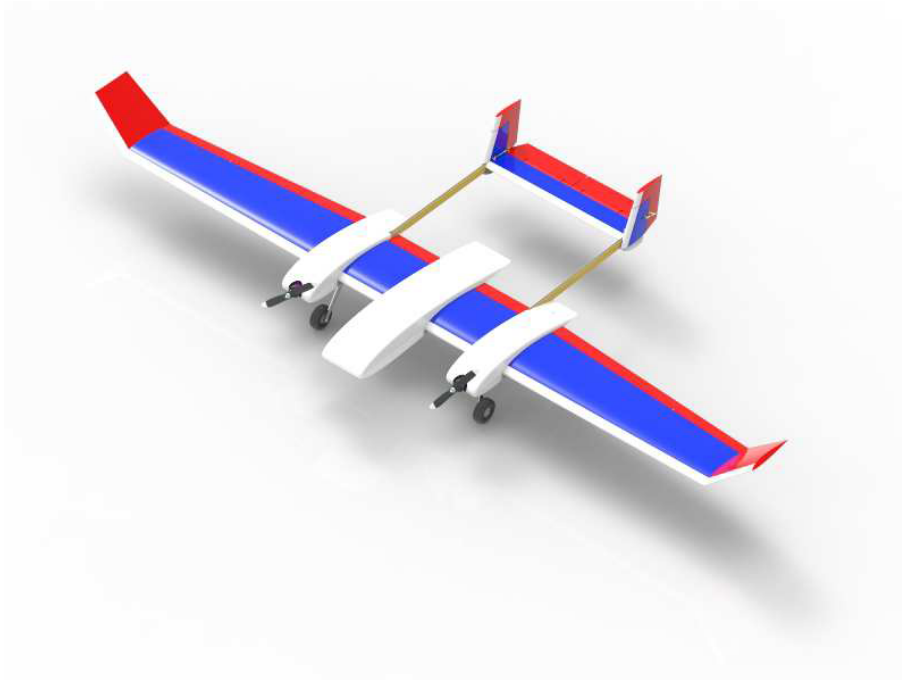


**Figure 1.2:** Realistic drawing of Sindy ([15]: title page)

me. The simulation consisted of a grid of feature points, and the goal was to use an ESKF-based algorithm to estimate the aircraft's state while flying along a predefined trajectory. I followed a gradual approach in the development process, starting with ideal conditions and incrementally introducing more realistic elements to the simulation. These included IMU- and measurement- noises, sensor biases, and pixelization. Firstly, I implemented the previously described filter with known 3-D coordinates of the measured feature points, but later a triangulation method was implemented called Linear Optimal Sine Triangulation (LOST). The next step involved the insertion of the LOST estimates into the ESKF framework.

The paper is structured as follows: Chapter 2 provides an introduction to several fundamental mathematical concepts that are crucial for comprehending our approach. In Chapter 3, the mathematical foundations of the filter are explained, and the steps of the filter are detailed. Chapter 4 focuses on the introduction of the applied triangulation method called LOST. Chapter 5 is devoted to introducing the integration issues of ESKF and LOST. Chapter 6 presents the estimation results in Matlab/Simulink environment. Finally, Chapter 7 offers a summary of the work, and highlights certain future development steps.

# CHAPTER 2

## MATHEMATICAL FOUNDATIONS

---

Before I would delve into the details of the visual-inertial relative navigation algorithm, it is important to establish theoretical foundations. This chapter summarizes the mathematical preliminaries that are essential for understanding how the algorithm works. It covers key concepts about coordinate systems and camera projection, and introduces an alternative method of rotation representation.

In my approach, filter-related mathematics uses four frames for the mathematical notation: Earth (E), node (N)-, body (B), and camera (C) frame. These are shown in Figure 2.1.

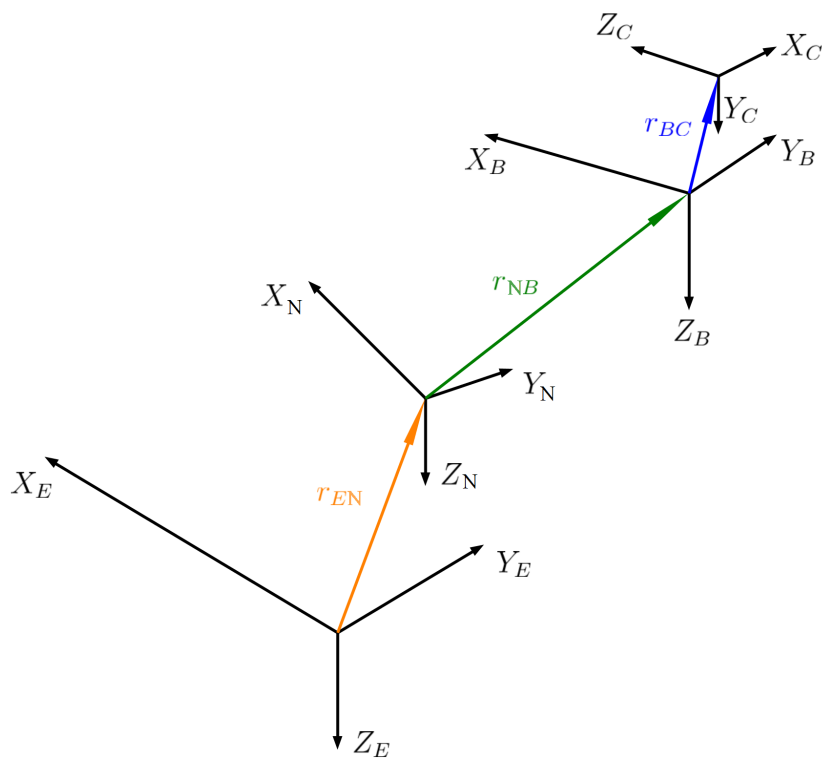


Figure 2.1: Applied coordinate systems

The Earth frame means an Earth fixed frame, and the North-East-Down (NED) coordinate system is chosen for this purpose in such UAV applications where the vehicle covers only a few kms. The node frame is a locally declared fixed frame, which usage is necessary for relative navigation methods since the filter produces estimates in this frame. The body- and camera frames are detailed in the following sections.

## 2.1 Navigation frames

The purpose of using different kinds of frames is to facilitate the kinematic modeling of UAVs. To effectively study UASs, it is crucial to comprehend the relative orientation and translation of different coordinate systems. Multiple frames are required for several reasons:

- The motion of the aircraft is most easily described in a body-fixed frame, however, Newton's equations of motion are derived relative to a fixed, inertial reference frame.
- The body-fixed frame is also used to express the aerodynamic forces and moments that affect the aircraft.
- On-board sensors such as accelerometers and gyroscopes measure concerning the body frame. This is essential in the case of strap-down IMUs since they provide accelerations and angular rates with respect to the body frame.
- Finally, the mission requirements of the aircraft, e.g. flight path require a global frame too.

### 2.1.1 North-East-Down reference frame

The NED coordinate system has emerged as a standard in UAV applications over limited distances, typically spanning a few kilometers. Notably, this reference frame is conventionally anchored to a stationary point on Earth, affording its use as an inertial reference frame in analytical computations. Consistent with its name, the NED system aligns its X-axis with the geographic north, its Y-axis

with the east, and its Z-axis points inwards to the Earth. Its X-Y plane is the local tangent plane of the Earth's ellipsoid.

The front end of relative navigation methods adopts the node coordinate system as an inertial frame, a crucial precondition for the functioning of the filter. The node frame remains locally fixed and undergoes redeclaration following each measurement. The back end of the system facilitates the derivation of global estimates, such as NED coordinates, utilizing the outcomes yielded by the filter.

### 2.1.2 Body frame

The body coordinate system is the most important besides the inertial frame. It appears directly in the kinematic equations, therefore it is crucial to understand properly how it is defined and what is the relation to the inertial frame. The origin is the center of the mass of the aircraft, and at this point, I would like to highlight the fact in almost every application the IMU is placed here. The axes of the body frame are defined as follows: the X-axis points out the nose of the aircraft, the Y-axis points out the right wing and the Z-axis points downwards.

Once the coordinate system has been defined, it is necessary to mention the relation to the inertial frame. The most commonly applied approach to obtain the orientation of the aircraft in the NED system is to express it with Euler angles which means three rotations one after another. Defining the Euler angles I use the same terminology as in [10], their approach is to introduce three additional coordinate systems: vehicle, vehicle-1, and vehicle-2. They are shown in Figure 2.2a-2.2d.

The vehicle frame is basically the NED coordinate system with shifted origin into the center of mass, vehicle-1 frame is rotated with the yaw angle ( $\psi$ ) around the Z-axis of vehicle frame, vehicle-2 frame is rotated with pitch angle ( $\theta$ ) around the Y-axis of vehicle-1 frame, and body frame is rotated with roll angle ( $\phi$ ) around the X-axis of vehicle-2 frame. To summarize, the resulting rotation can be defined as:

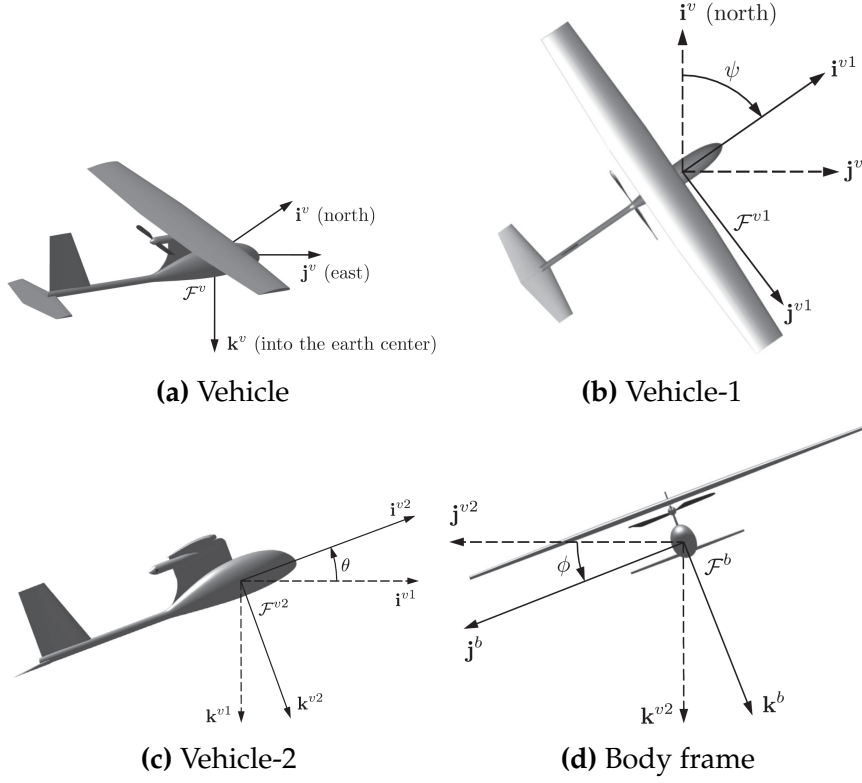


**Figure 2.2:** Frames to define Euler angles ([10]: pages 13-15, Figures 2.4-2.7)

$$\begin{aligned}
 \mathbf{R}_{BV}(\phi, \theta, \psi) &= \mathbf{R}_{BV_2}(x, \phi) \mathbf{R}_{V_2V_1}(y, \theta) \mathbf{R}_{V_1V}(z, \psi) \\
 &= \begin{bmatrix} C_\theta C_\psi & C_\theta S_\psi & -S_\theta \\ S_\phi S_\theta C_\psi - C_\phi S_\psi & S_\phi S_\theta S_\psi + C_\phi C_\psi & S_\phi C_\theta \\ C_\phi S_\theta C_\psi + S_\phi S_\psi & C_\phi S_\theta S_\psi - S_\phi C_\psi & C_\phi C_\theta \end{bmatrix}, \quad (2.1)
 \end{aligned}$$

where  $C_\alpha$  is shorthand for  $\cos(\alpha)$  and  $S_\alpha$  for  $\sin(\alpha)$ .

Finally, I would like to mention the usage of homogeneous transformation is widespread regarding vision-based applications, thanks to the fact it allows the calculation of three-dimensional (3D) coordinates from one frame to another with a single matrix multiplication. With known translation  $\mathbf{r}_{EB}$  and rotation ( $\mathbf{R}_{BE} \equiv \mathbf{R}_{BV}$ ) between the Earth frame (NED) and body frame, the homogeneous transformation can be expressed as:

$$\mathbf{H}_{BE} = \begin{bmatrix} \mathbf{R}_{BE} & \mathbf{r}_{EB} \\ \mathbf{0}^T & 1 \end{bmatrix} \quad (2.2)$$



The transformation can be applied as:

$$\mathbf{H}_{BE} = \begin{bmatrix} \mathbf{R}_{BE} & \mathbf{r}_{EB} \\ \mathbf{0}^T & 1 \end{bmatrix} \begin{bmatrix} \mathbf{v}_e \\ 1 \end{bmatrix} = \begin{bmatrix} \mathbf{R}_{BE}\mathbf{v}_e + \mathbf{r}_{EB} \\ 1 \end{bmatrix} \quad (2.3)$$

## 2.2 Camera frames

It is important to say a few words about camera-related frames and transformation in view of the fact that, camera pictures are used to improve navigation. I would like to clarify that, we distinguish between a camera- and an image coordinate system. This means that a point with known coordinates in the Earth frame can be projected onto the image plane with two operations: a transformation is needed from the Earth frame to the camera system and after that, a projection is needed.

### 2.2.1 Camera system

It is very important to determine the transformation from body-to-camera system with sufficient accuracy. Generally, the camera is not placed in the body center, therefore the transformation first requires a translation with  $\mathbf{r}_{BC}$ . Since navigation happens with respect to the surroundings an at least partially downward-facing camera is mandatory, which means a rotation is needed around the Y-axis of the body frame. Furthermore, the axes of the camera system are defined differently, than the axes of the body frame, therefore an additional operation is essential to change the axes. Figure 2.3 shows why the swapping is needed: almost every application defines the axes of the camera system as follows: the X-axis points to the right, Y-axis points to the bottom and Z-axis points out of the principal point of the image.

It means that the basis vectors of the rotated body frame should be transformed as outlined below:  $\vec{i}'_b = \vec{k}_c$ ,  $\vec{j}'_b = \vec{i}_c$  and  $\vec{k}'_b = \vec{j}_c$ , the transformation from body-to-

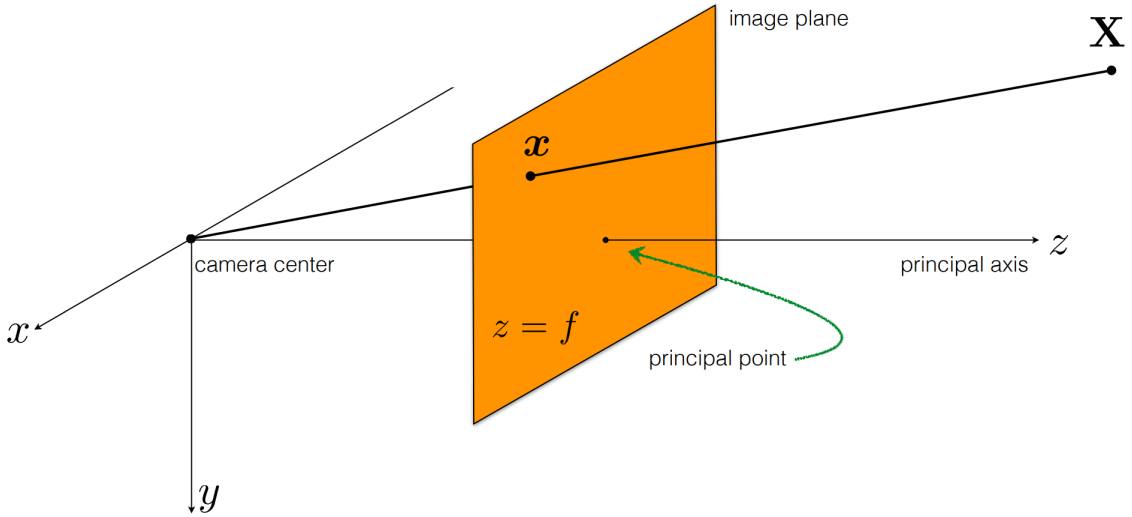


Figure 2.3: Camera and image system ([16]: page 7)

camera frame:

$$\begin{aligned}
 \mathbf{T}_{CB} = \mathbf{S}\mathbf{R}_{CB}(y, \beta) &= \begin{bmatrix} 0 & 1 & 0 \\ 0 & 0 & 1 \\ 1 & 0 & 0 \end{bmatrix} \begin{bmatrix} \cos(\beta) & 0 & -\sin(\beta) \\ 0 & 1 & 0 \\ \sin(\beta) & 0 & \cos(\beta) \end{bmatrix} \\
 &= \begin{bmatrix} 0 & 1 & 0 \\ \sin(\beta) & 0 & \cos(\beta) \\ \cos(\beta) & 0 & -\sin(\beta) \end{bmatrix}, \tag{2.4}
 \end{aligned}$$

where  $\mathbf{S}$  stands for the axes swapping transformation, and  $\beta$  is the angle between the camera and the body. Considering the translation the homogeneous transformation can be written in the form of:

$$\mathbf{H}_{CB} = \begin{bmatrix} \mathbf{T}_{CB} & \mathbf{r}_{BC} \\ \mathbf{0}^T & 1 \end{bmatrix} \tag{2.5}$$

## 2.2.2 Pinhole camera projection

Here and now, every known point in the Earth frame can be transformed into the camera system with the usage of (2.2) and (2.5). The next task is to determine the pixel coordinates of the point in question, and this requires a projection  $h(\cdot)$ . For the simulation, the most simple model was chosen, the pinhole camera projection

model. The pinhole model framework describes the aperture of the camera as a point, therefore the lens distortion errors are neglected. As it can be seen in Figure 2.3, the model only requires two parameters:

1. The focal length ( $f$ ) which shows the distance between the camera center and the image plane.
2. The second parameter is the principal point which is typically near the center of the image, however, it is a bit shifted in real cameras.

With the mentioned parameters, the transformation includes the normalization of points with their distance from the camera center and the projection onto the image plane. In the pinhole framework, the transformation of the normalized points can be specified with a camera matrix, which can be derived from pinhole parameters:

$$\mathbf{K} = \begin{bmatrix} f & 0 & p_x \\ 0 & f & p_y \\ 0 & 0 & f \end{bmatrix} \quad (2.6)$$

Using (2.6) the whole projection is defined as:

$$h(\mathbf{p}_c) = \mathbf{K} \frac{\mathbf{p}_c}{z_c} = \begin{bmatrix} f & 0 & p_x \\ 0 & f & p_y \\ 0 & 0 & f \end{bmatrix} \begin{bmatrix} \frac{x_c}{z_c} \\ \frac{y_c}{z_c} \\ 1 \end{bmatrix} = \begin{bmatrix} f \frac{x_c}{z_c} + p_x \\ f \frac{y_c}{z_c} + p_y \\ f \end{bmatrix} = \begin{bmatrix} u \\ v \\ f \end{bmatrix} \quad (2.7)$$

As a final point, I would like to emphasize that the (2.7) transformation can determine the image coordinates of every three-dimensional point, but a real camera has limitations which can be described either with the image size ( $W, H$ ) or the FOV angles.

## 2.3 Quaternions

Before embarking into the ESKF, it is worth mentioning a few words about quaternions. Originally formulated in [17] by Sir William Rowan in the 19th

century. Nowadays, quaternions have found extensive applications in various domains, including computer graphics, robotics, and aerospace engineering.

In this paper, I adopt the same mathematical representation for quaternions as described in [18]. Quaternions belong to the extended complex number space, which includes two additional imaginary units, namely  $j$  and  $k$ , in addition to the real and imaginary unit  $i$ . As a result, quaternions can be represented by four-component vectors:

$$\mathbf{q} = a + b\mathbf{i} + c\mathbf{j} + d\mathbf{k} = \begin{bmatrix} a & b & c & d \end{bmatrix}^T = \begin{bmatrix} q_w \\ \mathbf{q}_v \end{bmatrix}, \quad (2.8)$$

where  $\mathbf{q}$  is a quaternion with  $a$ ,  $b$ ,  $c$ , and  $d$  parameters. The quaternion can be expressed as a column vector or as a combination of the scalar component  $q_w$  and the vector component  $\mathbf{q}_v$ .

It is noticeable that, while regular complex numbers of unit length ( $\mathbf{z} = e^{i\theta}$ ) are able to encode rotations in the 2D space, quaternions of unit length ( $\mathbf{q} = e^{(u_x i + u_y j + u_z k)\theta/2}$ ) can encode rotations in the 3D space. These quaternions can always be written in the form:

$$\mathbf{q} = \begin{bmatrix} \cos\left(\frac{\theta}{2}\right) \\ \sin\left(\frac{\theta}{2}\right) \mathbf{u} \end{bmatrix}, \quad (2.9)$$

where  $\mathbf{u}$  is the rotation axis and  $\theta$  is the angle of the rotation. The rotation can be performed on the 3D vector  $\mathbf{v}$  by the following operation:

$$\begin{bmatrix} 0 \\ \mathbf{v}' \end{bmatrix} = \mathbf{q} \otimes \begin{bmatrix} 0 \\ \mathbf{v} \end{bmatrix} \otimes \mathbf{q}^*, \quad (2.10)$$

where  $\otimes$  is the Hamiltonian-quaternion multiplication, and  $\mathbf{q}^*$  is the conjugate of  $\mathbf{q}$ .

The composition of two rotation, described by  $\mathbf{q}_{AB}$  and  $\mathbf{q}_{BC}$  quaternions can also be evaluated using quaternion product:

$$\mathbf{q}_{AC} = \mathbf{q}_{AB} \otimes \mathbf{q}_{BC} \quad (2.11)$$

Further definitions and important formulas relevant to this paper are provided in Appendix A.

Finally, I aim to justify the significance of quaternions in the field of computer calculations. The first striking benefit is that quaternions offer a compact representation of rotations, requiring only 4 parameters. In contrast, rotation matrices necessitate 9 parameters. Another advantage of quaternions is their ability to ensure more stable and accurate computations by avoiding singularities and mitigating the issue of gimbal lock, which can occur both for rotation matrices and Euler angles.

# CHAPTER 3

## INTRODUCTION OF THE APPLIED FILTER TECHNIQUE

---

Upon laying down essential mathematical foundations, the subsequent focus shifts toward introducing the chosen filter technique. In visual-inertial projects, various approaches are available to filter measurements and estimate the system's state. Many of these approaches are a modified Kalman filter. The basics of the implemented filter are based on the ESKF, which stands as a remarkable method for filtering and estimating nonlinear systems. The basic algorithm is taken from [18], but with three major differences:

1. I didn't insert the gravitational constant ( $\mathbf{g}$ ) in the state vectors  $\mathbf{x}, \delta\mathbf{x}$  to estimate UAVs usually fly small distances and the gravitational acceleration can be assumed constant.
2. The velocity vector  $\mathbf{v}$  is body-fixed in my approach, making it  $\mathbf{v}_b$ . On the contrary, the mentioned literature uses an inertial frame fixed velocity vector.
3. In their method, the rotation described by quaternion  $\mathbf{q}$  and rotation matrix  $\mathbf{R}\{\mathbf{q}\} \equiv \mathbf{R}^{-1}$  stands for the body-to-earth rotation, while in this paper rotation stands for the inverse transformation, earth-to-body transformation to match the conventional Euler angle representation of rotation commonly applied in aerospace. This impacts the formulation of the mathematical equations, but in most cases, the equations have symmetrical properties.

---

<sup>1</sup>In this paper,  $\mathbf{R}\{\mathbf{q}\}$  denotes the rotation matrix obtained from quaternion.

## 3.1 Error-state kinematics

In IMU-driven systems the goal is to create a filter framework, that integrates the accelerometer and gyrometer readings considering their bias and measurement noise. As I previously detailed the IMU measurements only themselves cause drift in their estimate, therefore they should be fused with absolute position readings such as GPS or vision.

One of the tools which can be used for this purpose is the ESKF, which has multiple advantages if applied for nonlinear systems:

- The error state always operates close to the actual system state, thus the linear Kalman filter approach can be applied to the error-state.
- All second-order products are negligible because the error-state always remains small. This makes the computation of Jacobians very easy and fast.
- The dynamics of the error-state are slow, due to all large-signal dynamics being integrated into the nominal-state. This results in a highly beneficial property: the KF corrections can be applied at a lower rate, than the predictions.

### 3.1.1 Kalman filter states for IMU driven systems

The objective is to estimate the position of the aircraft, which requires to use of the kinematic equations of the aircraft. The kinematics expresses the relationships among position, orientation, velocity, acceleration, and angular velocity. Whereas acceleration and angular velocity are utilized as IMU measurements, the state includes position, velocity, and orientation. Moreover, it is supplemented by estimating the biases of the sensors.

The position and orientation of the body are expressed in a fixed frame, which is usually the node frame in relative navigation projects, but currently, the developed system doesn't implement a backend, therefore there is no purpose for the usage of the node frame. So from now on the localization frame is considered

NED. On the contrary, the velocity and the biases are body-frame fixed, which results in the state vector:

$$\mathbf{x} = \begin{bmatrix} \mathbf{p}_n \\ \mathbf{q}_n \\ \mathbf{v}_b \\ \boldsymbol{\beta}_a \\ \boldsymbol{\beta}_\omega \end{bmatrix} \quad (3.1)$$

### 3.1.2 ESKF states

In the ESKF framework, there are three different states: true- ( $\mathbf{x}_t$ ), nominal- ( $\mathbf{x}$ ), and error-state ( $\delta\mathbf{x}$ ). In Table 3.1 all of the ESKF variables are summarized.

True	Nominal	Error	Composition	Noise	Measured
$\mathbf{p}_{n,t}$	$\mathbf{p}_n$	$\delta\mathbf{p}_n$	$\mathbf{p}_{n,t} = \mathbf{p}_n + \delta\mathbf{p}_n$		
$\mathbf{q}_{n,t}$	$\mathbf{q}_n$	$\delta\mathbf{q}_n \approx \begin{bmatrix} 1 \\ \frac{1}{2}\delta\boldsymbol{\theta} \end{bmatrix}$	$\mathbf{q}_{n,t} = \delta\mathbf{q} \otimes \mathbf{q}_n$		
$\mathbf{v}_{b,t}$	$\mathbf{v}_b$	$\delta\mathbf{v}_b$	$\mathbf{v}_{b,t} = \mathbf{v}_b + \delta\mathbf{v}_b$		
$\boldsymbol{\beta}_{a,t}$	$\boldsymbol{\beta}_a$	$\delta\boldsymbol{\beta}_a$	$\boldsymbol{\beta}_{a,t} = \boldsymbol{\beta}_a + \delta\boldsymbol{\beta}_a$	$\boldsymbol{\eta}_{\beta_a}$	
$\boldsymbol{\beta}_{\omega,t}$	$\boldsymbol{\beta}_\omega$	$\delta\boldsymbol{\beta}_\omega$	$\boldsymbol{\beta}_{\omega,t} = \boldsymbol{\beta}_\omega + \delta\boldsymbol{\beta}_\omega$	$\boldsymbol{\eta}_{\beta_\omega}$	
$\mathbf{R}_t$	$\mathbf{R}$	$\delta\mathbf{R} = e^{\begin{bmatrix} \delta\boldsymbol{\theta} \end{bmatrix}_\times}$	$\mathbf{R}_t = \delta\mathbf{R}\mathbf{R}$		
$\mathbf{a}_t$				$\boldsymbol{\eta}_a$	$\mathbf{a}_m$
$\boldsymbol{\omega}_t$				$\boldsymbol{\eta}_\omega$	$\boldsymbol{\omega}_m$

**Table 3.1:** ESKF states and inputs

The states are divided in such a way that the large-signal dynamics are assigned to the nominal state, while the small-signal dynamics are assigned to the error state. A few comments on the table:

- The relation between the error- quaternion and rotation vector was presented, using the formula defined in Appendix A.1, then approximating cosine and sine as above, because  $\delta\boldsymbol{\theta}$  is always near 0.



- The body referenced measurements are  $\mathbf{a}_m$  and  $\boldsymbol{\omega}_m$ . Their values are captured as noisy IMU measurements, therefore:

$$\begin{aligned}\mathbf{a}_m &= \mathbf{a}_t - \mathbf{R}_t \mathbf{g} + \boldsymbol{\beta}_{a,t} + \boldsymbol{\eta}_a \\ \boldsymbol{\omega}_m &= \boldsymbol{\omega}_t + \boldsymbol{\beta}_{\omega,t} + \boldsymbol{\eta}_\omega\end{aligned}\quad (3.2)$$

From above the true values can be obtained, and substituting nominal- and error- values into true variables:

$$\begin{aligned}\mathbf{a}_t &= \overbrace{\mathbf{a}_m - \boldsymbol{\beta}_a}^{\mathbf{a}} + \mathbf{R}\mathbf{g} - \overbrace{\delta\boldsymbol{\beta}_a - \boldsymbol{\eta}_a}^{\delta\mathbf{a}} \\ \boldsymbol{\omega}_t &= \overbrace{\boldsymbol{\omega}_m - \boldsymbol{\beta}_\omega}^{\boldsymbol{\omega}} - \overbrace{\delta\boldsymbol{\beta}_\omega - \boldsymbol{\eta}_\omega}^{\delta\boldsymbol{\omega}}\end{aligned}\quad (3.3)$$

- The biases small-signal dynamics  $\delta\boldsymbol{\beta}_a, \delta\boldsymbol{\beta}_\omega$  are represented with Gaussian white noises  $\boldsymbol{\eta}_{\beta_a}, \boldsymbol{\eta}_{\beta_\omega}$ , just like the measurement noises  $\boldsymbol{\eta}_a, \boldsymbol{\eta}_\omega$ .
- The true rotation matrix can be approximated by composing the nominal rotation matrix with power series because  $\delta\mathbf{R}$  can be written in Taylor-series. The (3.4) approximation is detailed in B.1, but the formula is provided here, therefore neglecting the second- and higher-order terms, it yields:

$$\mathbf{R}_t = \delta\mathbf{R}\mathbf{R} = \left( \mathbf{I} + \begin{bmatrix} \delta\boldsymbol{\theta} \end{bmatrix}_\times \right) \mathbf{R} + O(\|\delta\boldsymbol{\theta}\|^2) \quad (3.4)$$

## True-state

The dynamics of the true state can be described by the following equations:

$$\dot{\mathbf{p}}_{n,t} = \mathbf{R}_t^T \mathbf{v}_{b,t} \quad (3.5a)$$

$$\dot{\mathbf{q}}_{n,t} = \frac{1}{2} \begin{bmatrix} 0 \\ -(\boldsymbol{\omega}_m - \boldsymbol{\beta}_{\omega,t} - \boldsymbol{\eta}_\omega) \end{bmatrix} \otimes \mathbf{q}_{n,t} \quad (3.5b)$$

$$\dot{\mathbf{v}}_{b,t} = \mathbf{a}_m - \boldsymbol{\beta}_{a,t} - \boldsymbol{\eta}_a + \mathbf{R}_t \mathbf{g} + \begin{bmatrix} \mathbf{v}_{b,t} \end{bmatrix}_\times (\boldsymbol{\omega}_m - \boldsymbol{\beta}_{\omega,t} - \boldsymbol{\eta}_\omega) \quad (3.5c)$$

$$\dot{\boldsymbol{\beta}}_{a,t} = \boldsymbol{\eta}_{\beta_a} \quad (3.5d)$$

$$\dot{\beta}_{\omega,t} = \eta_{\beta\omega} \quad (3.5e)$$

The (3.5b) is the time derivative formula of quaternion, and detailed in Appendix A.2. The (3.5c) also requires some explanation because this equation applies the rule of vector derivative in rotating frames compared to an inertial frame:

$$\frac{d}{dt_i} \mathbf{v} = \frac{d}{dt_b} \mathbf{v} + \boldsymbol{\omega}_{b/i} \times \mathbf{v} \Rightarrow \frac{d}{dt_b} \mathbf{v} = \frac{d}{dt_i} \mathbf{v} + \mathbf{v} \times \boldsymbol{\omega}_{b/i}, \quad (3.6)$$

where the anti-commutative property of the cross product was used ( $\boldsymbol{\omega}_{b/i} \times \mathbf{v} = -\mathbf{v} \times \boldsymbol{\omega}_{b/i}$ ). In (3.5c), the cross product is expressed in matrix form with the skew operator  $[\cdot]_{\times}$ , which can be constructed as:

$$[\mathbf{a}]_{\times} \triangleq \begin{bmatrix} 0 & -a_z & a_y \\ a_z & 0 & -a_x \\ -a_y & a_x & 0 \end{bmatrix} \quad (3.7)$$

## Nominal-state

The nominal-state corresponds to the modeled system without noises and perturbations:

$$\dot{\mathbf{p}}_n = \mathbf{R}^T \mathbf{v}_b \quad (3.8a)$$

$$\dot{\mathbf{q}}_n = \frac{1}{2} \begin{bmatrix} 0 \\ -\boldsymbol{\omega} \end{bmatrix} \otimes \mathbf{q}_n \quad (3.8b)$$

$$\dot{\mathbf{v}}_b = \mathbf{a} + \mathbf{R}\mathbf{g} + [\mathbf{v}_b]_{\times} \boldsymbol{\omega} \quad (3.8c)$$

$$\dot{\beta}_{a,t} = 0 \quad (3.8d)$$

$$\dot{\beta}_{\omega,t} = 0 \quad (3.8e)$$

These equations reflect the dynamics of the system with slowly varying biases, which is beneficial because allows the integration of large-signal dynamics into the nominal-state.

## Error-state

The error-state equations are derived by using the previously defined true- and nominal-state equations. The equations governing the error-state are as follows:

$$\delta \dot{\mathbf{p}}_n = \mathbf{R}^T \delta \mathbf{v}_b + \mathbf{R}^T \left[ \mathbf{v}_b \right]_{\times} \delta \boldsymbol{\theta} \quad (3.9a)$$

$$\delta \dot{\boldsymbol{\theta}} = - \left[ \boldsymbol{\omega}_m + \boldsymbol{\beta}_\omega \right]_{\times} \delta \boldsymbol{\theta} + \delta \boldsymbol{\beta}_\omega + \boldsymbol{\eta}_\omega \quad (3.9b)$$

$$\begin{aligned} \delta \dot{\mathbf{v}}_b = & - \left[ \mathbf{R}\mathbf{g} \right]_{\times} \delta \boldsymbol{\theta} - \left[ \boldsymbol{\omega}_m - \boldsymbol{\beta}_\omega \right]_{\times} \delta \mathbf{v}_b - \delta \boldsymbol{\beta}_a - \left[ \mathbf{v}_b \right]_{\times} \delta \boldsymbol{\beta}_\omega \\ & - \boldsymbol{\eta}_a - \left[ \mathbf{v}_b \right]_{\times} \boldsymbol{\eta}_\omega \end{aligned} \quad (3.9c)$$

$$\delta \dot{\boldsymbol{\beta}}_a = \boldsymbol{\eta}_{\beta_a} \quad (3.9d)$$

$$\delta \dot{\boldsymbol{\beta}}_\omega = \boldsymbol{\eta}_{\beta_\omega} \quad (3.9e)$$

The calculations are detailed in Appendix B.2.

### 3.1.3 Error-state kinematics in discrete time

The previous equations are defined in continuous-time, but computer implementations use a discrete-time model. To incorporate discrete time intervals  $\Delta t > 0$ , the differential equations mentioned earlier must be transformed into difference equations through integration.

The integration method may vary, since in certain cases, exact closed-form solutions can be utilized, while in other cases, numerical integration techniques with varying degrees of accuracy may be employed. Generally, we could say the equations have a deterministic part related to state dynamics and control, on the other hand, there is a stochastic part related to perturbations and noises. In this case,

the same method will be presented as in [18]: the deterministic part integrated according to the ZOH method, and the stochastic part modeled as random impulses applied to the velocity, orientation, and bias estimates. This results in the nominal-state equations:

$$\mathbf{p}_{n,k+1} = \mathbf{p}_{n,k} + \mathbf{R}^T \mathbf{v}_{b,k} \Delta t + \frac{1}{2} \mathbf{R}^T \left( \mathbf{a}_k + \mathbf{R} \mathbf{g} + \left[ \mathbf{v}_{b,k} \right]_{\times} \boldsymbol{\omega}_k \right) \Delta t^2 \quad (3.10a)$$

$$\mathbf{q}_{n,k+1} = \mathbf{q} \{ -(\boldsymbol{\omega}_m - \boldsymbol{\beta}_\omega) \Delta t \} \otimes \mathbf{q}_{n,k} \quad (3.10b)$$

$$\mathbf{v}_{b,k+1} = \mathbf{v}_{b,k} + \left( \mathbf{a}_k + \mathbf{R} \mathbf{g} + \left[ \mathbf{v}_{b,k} \right]_{\times} \boldsymbol{\omega}_k \right) \Delta t \quad (3.10c)$$

$$\boldsymbol{\beta}_{a,k+1} = \boldsymbol{\beta}_{a,k} \quad (3.10d)$$

$$\boldsymbol{\beta}_{\omega,k+1} = \boldsymbol{\beta}_{\omega,k} \quad (3.10e)$$

The position is integrated both from velocity and acceleration, and the rotation from angular velocity. The last one is given in a closed form assuming that the angular velocity is constant during the sampling interval. Using the same integration approach complemented by the integration of the stochastic part, the error-state equations result as:

$$\delta \mathbf{p}_{n,k+1} = \delta \mathbf{p}_{n,k} + \mathbf{R}^T \left( \delta \mathbf{v}_{b,k} + \left[ \mathbf{v}_{b,k} \right]_{\times} \delta \boldsymbol{\theta}_k \right) \Delta t \quad (3.11a)$$

$$\delta \boldsymbol{\theta}_{k+1} = \mathbf{R} \{ -(\boldsymbol{\omega}_{m,k} - \boldsymbol{\beta}_{\omega,k}) \Delta t \} \delta \boldsymbol{\theta}_k + \delta \boldsymbol{\beta}_{\omega,k} \Delta t + \boldsymbol{\theta}_{i,k} \quad (3.11b)$$

$$\begin{aligned} \delta \mathbf{v}_{b,k+1} = \delta \mathbf{v}_{b,k} + \left( - \left[ \mathbf{R} \mathbf{g} \right]_{\times} \delta \boldsymbol{\theta}_k - \left[ \boldsymbol{\omega}_{m,k} - \boldsymbol{\beta}_{\omega,k} \right]_{\times} \delta \mathbf{v}_{b,k} \right. \\ \left. - \delta \boldsymbol{\beta}_{a,k} - \left[ \mathbf{v}_{b,k} \right]_{\times} \delta \boldsymbol{\beta}_{\omega,k} \right) \Delta t - \left[ \mathbf{v}_{b,k} \right]_{\times} \boldsymbol{\theta}_{i,k} - \mathbf{v}_{b,i,k} \end{aligned} \quad (3.11c)$$

$$\delta \boldsymbol{\beta}_{a,k+1} = \delta \boldsymbol{\beta}_{a,k} + \mathbf{a}_{i,k} \quad (3.11d)$$

$$\delta \boldsymbol{\beta}_{\omega,k+1} = \delta \boldsymbol{\beta}_{\omega,k} + \boldsymbol{\omega}_{i,k} \quad (3.11e)$$

$\boldsymbol{\theta}_i$ ,  $\mathbf{v}_{b,i}$ ,  $\mathbf{a}_i$  and  $\boldsymbol{\omega}_i$  are the random impulses which form the stochastic part of the equation. Hence, they are modeled as Gaussian white noises, the negative sign freely can be changed to a positive. Their covariance matrices are integrated as

(see [18] Appendix E for details):

$$\begin{aligned}
\Theta_i &= \sigma_{\eta_\omega}^2 \Delta t^2 \mathbf{I} \\
\mathbf{V}_i &= \sigma_{\eta_a}^2 \Delta t^2 \mathbf{I} \\
\mathbf{A}_i &= \sigma_{\beta_a}^2 \Delta t \mathbf{I} \\
\mathbf{\Omega}_i &= \sigma_{\beta_\omega}^2 \Delta t \mathbf{I}
\end{aligned} \tag{3.12}$$

## 3.2 Measurement equation

The measurement equation is based on the fundamental concept that the system can acquire pixel coordinates of feature points as measurements. In order to form the residual, the predicted pixel coordinates must be determined for each feature point. This can be accomplished through the application of the pinhole equation (2.7), which leads to:

$$h(\mathbf{T}_{CB}(\mathbf{R}_{BE}(\mathbf{p}_n^f - \mathbf{p}_n^b) - \mathbf{p}_b^c)) = h(\mathbf{p}_c^f) = \begin{bmatrix} u \\ v \\ f \end{bmatrix}, \tag{3.13}$$

where  $\mathbf{p}_n^f$  denotes the feature position in NED frame,  $\mathbf{p}_c^f$  means the feature position in camera frame and  $\mathbf{p}_b^c$  describes the camera origin in body frame. The transformation above requires the usage of both the state  $(\mathbf{p}_n^b, \mathbf{q}_n^b)$  and  $\mathbf{p}_n^f$ , thus, linearizing the measurement equation yields two Jacobians, but in this chapter, only the Jacobian with respect to the state is discussed.

## 3.3 ESKF framework

The ESKF is a special version of the Kalman filter, that contains two state vectors: one for the nominal- ( $\mathbf{x}_k$ ) and the other for the error-state ( $\delta\mathbf{x}_k$ ) vector. The system

is governed by the input  $\mathbf{u}_k$  and the noise perturbations  $\mathbf{i}$ :

$$\mathbf{x}_k = \begin{bmatrix} \mathbf{p}_{n,k} \\ \mathbf{q}_{n,k} \\ \mathbf{v}_{b,k} \\ \boldsymbol{\beta}_{a,k} \\ \boldsymbol{\beta}_{\omega,k} \end{bmatrix}, \quad \delta\mathbf{x}_k = \begin{bmatrix} \delta\mathbf{p}_{n,k} \\ \delta\boldsymbol{\theta}_k \\ \delta\mathbf{v}_{b,k} \\ \delta\boldsymbol{\beta}_{a,k} \\ \delta\boldsymbol{\beta}_{\omega,k} \end{bmatrix}, \quad \mathbf{u}_k = \begin{bmatrix} \mathbf{a}_{m,k} \\ \boldsymbol{\omega}_{m,k} \end{bmatrix}, \quad \mathbf{i} = \begin{bmatrix} \boldsymbol{\theta}_i \\ \mathbf{v}_i \\ \mathbf{a}_i \\ \boldsymbol{\omega}_i \end{bmatrix} \quad (3.14)$$

### 3.3.1 Prediction step

One of the best properties of the ESKF framework is that during the prediction steps the nominal state can be calculated by the original nonlinear equations (3.10), but the error-state has to be linearized. The transition- ( $\mathbf{F}_x$ ) and noise matrix ( $\mathbf{F}_i$ ) can be derived from (3.11), where  $\delta\mathbf{x}_{k+1} = f(\delta\mathbf{x}_k)$ :

$$\mathbf{F}_x = \frac{\partial f}{\partial \delta\mathbf{x}_k} = \begin{bmatrix} \mathbf{I} & \mathbf{R}^T [\mathbf{v}_{b,k}]_{\times} \Delta t & \mathbf{R}^T \Delta t & \mathbf{0} & \mathbf{0} \\ \mathbf{0} & \mathbf{R}\{-(\boldsymbol{\omega}_{m,k} - \boldsymbol{\beta}_{\omega,k})\Delta t\} & \mathbf{0} & \mathbf{0} & \mathbf{I}\Delta t \\ \mathbf{0} & -[\mathbf{R}\mathbf{g}]_{\times} \Delta t & \mathbf{I} - [\boldsymbol{\omega}_{m,k} - \boldsymbol{\beta}_{\omega,k}]_{\times} \Delta t & -\mathbf{I}\Delta t & -[\mathbf{v}_{b,k}]_{\times} \Delta t \\ \mathbf{0} & \mathbf{0} & \mathbf{0} & \mathbf{I} & \mathbf{0} \\ \mathbf{0} & \mathbf{0} & \mathbf{0} & \mathbf{0} & \mathbf{I} \end{bmatrix} \quad (3.15)$$

$$\mathbf{F}_i = \frac{\partial f}{\partial \mathbf{i}} = \begin{bmatrix} \mathbf{0} & \mathbf{0} & \mathbf{0} & \mathbf{0} \\ \mathbf{I} & \mathbf{0} & \mathbf{0} & \mathbf{0} \\ -[\mathbf{v}_{b,k}]_{\times} & -\mathbf{I} & \mathbf{0} & \mathbf{0} \\ \mathbf{0} & \mathbf{0} & \mathbf{I} & \mathbf{0} \\ \mathbf{0} & \mathbf{0} & \mathbf{0} & \mathbf{I} \end{bmatrix}, \quad (3.16)$$

where  $\mathbf{I}, \mathbf{0} \in \mathbb{R}^{3 \times 3}$ . Now the error-state dynamic is:

$$\delta\mathbf{x}_{k+1} = \mathbf{F}_x \delta\mathbf{x}_k + \mathbf{F}_i \mathbf{i} \quad (3.17)$$

Using formulas from above and denote equations in (3.10) with  $f(\cdot)$  the prediction step involves:

$$\mathbf{x}_{k+1} = f(\mathbf{x}_k, \mathbf{u}_k) \quad (3.18a)$$

$$\delta \hat{\mathbf{x}}_{k+1} = \mathbf{F}_x \delta \hat{\mathbf{x}}_k \quad (3.18b)$$

$$\mathbf{P}_{k+1} = \mathbf{F}_x \mathbf{P}_k \mathbf{F}_x^T + \mathbf{F}_i \mathbf{Q}_i \mathbf{F}_i^T \quad (3.18c)$$

Here,  $\delta \hat{\mathbf{x}}$  is the mean of the error-state, therefore  $\delta \mathbf{x} \sim \mathcal{N}(\delta \hat{\mathbf{x}}, \mathbf{P})$ . It is noteworthy to mention that the error-state is modeled with Gaussian white noise, therefore its prediction is always 0.

### 3.3.2 Update step

Here, I just focus on how the measurement Jacobian of the error-state is calculated. The most straightforward approach to do that for a feature point involves the utilization of the chain rule.

$$\mathbf{H}_x = \frac{\partial h(\mathbf{p}_c^f)}{\partial \delta \mathbf{x}} = \frac{\partial h(\mathbf{p}_c^f)}{\partial \mathbf{p}_c^f} \frac{\partial \mathbf{p}_c^f}{\partial \mathbf{x}_t} \frac{\partial \mathbf{x}_t}{\partial \delta \mathbf{x}} = \mathbf{J} \mathbf{P}_{x_t} \mathbf{X}_{\delta x}, \quad (3.19)$$

where  $h$  is the nonlinear transformation that projects  $\mathbf{p}_c^f$  onto the image plane.

### Jacobian of the pinhole model with respect to feature point

The Jacobian of the projection is calculated by linearizing (2.7), whereas the transformation results in a 3-element column vector, and the point has 3 coordinates the Jacobian should be a  $3 \times 3$  matrix, but the last row leads to only zeros which are not very useful, therefore it is neglected:

$$\mathbf{J} = \begin{bmatrix} \frac{\partial h_1(\mathbf{p}_c^f)}{\partial x} & \frac{\partial h_1(\mathbf{p}_c^f)}{\partial y} & \frac{\partial h_1(\mathbf{p}_c^f)}{\partial z} \\ \frac{\partial h_2(\mathbf{p}_c^f)}{\partial x} & \frac{\partial h_2(\mathbf{p}_c^f)}{\partial y} & \frac{\partial h_2(\mathbf{p}_c^f)}{\partial z} \end{bmatrix} = \begin{bmatrix} \frac{f}{z} & 0 & -\frac{fx}{z^2} \\ 0 & \frac{f}{z} & -\frac{fy}{z^2} \end{bmatrix} \Big|_{\mathbf{p}_c^f} \quad (3.20)$$

## Jacobian of the feature point with respect to the true-state

The next step is to determine the derivative of  $\mathbf{p}_c^f$  by the true-state. Since the feature point is known in the localization frame, its transformation into the camera frame should be considered:

$$\frac{\partial \mathbf{p}_c^f}{\partial \mathbf{x}_t} = \frac{\partial \mathbf{T}_{CB} \mathbf{R}\{\mathbf{q}_n^b\} (\mathbf{p}_n^f - \mathbf{p}_n^b)}{\partial \mathbf{x}_t}, \quad (3.21)$$

Here,  $\mathbf{p}_n^b$  and  $\mathbf{q}_n^b$  are elements from the state-vector, just they got superscripts to clearly mark they describe the position and orientation of the body frame. It can be seen that there is no other state parameter in the expression, therefore further derivatives result in  $\mathbf{0}_{3 \times 3}$  matrices. The derivative by  $\mathbf{p}_n^b$  can be determined easily:

$$\frac{\partial \mathbf{p}_c^f}{\partial \mathbf{p}_n^b} = -\mathbf{T}_{CB} \mathbf{R}\{\mathbf{q}_n^b\} \quad (3.22)$$

Calculating the derivative by the quaternion is tricky. Initially, the quaternion rotation formula needs to be employed on (3.21), then the derivative should be decomposed using the chain rule into separate components: one with respect to the vector and the other with respect to the quaternion:

$$\begin{aligned} \frac{\partial \mathbf{p}_c^f}{\partial \mathbf{q}_n} &= \left. \frac{\partial \mathbf{q}_{CB} \otimes \mathbf{q}_n \otimes (\mathbf{p}_n^f - \mathbf{p}_n^b) \otimes \mathbf{q}_n^* \otimes \mathbf{q}_{CB}^*}{\partial \mathbf{q}_n} \right|_{\mathbf{a}=\mathbf{p}_n^f - \mathbf{p}_n^b} \\ &= \frac{\partial \mathbf{q}_{CB} \otimes (\mathbf{q}_n \otimes \mathbf{a} \otimes \mathbf{q}_n^*) \otimes \mathbf{q}_{CB}^*}{\partial \mathbf{q}_n \otimes \mathbf{a} \otimes \mathbf{q}_n^*} \frac{\partial \mathbf{q}_n \otimes \mathbf{a} \otimes \mathbf{q}_n^*}{\partial \mathbf{q}_n} \end{aligned} \quad (3.23)$$

Using results from Appendices A.3 and A.4, the outcome is:

$$\frac{\partial \mathbf{p}_c^f}{\partial \mathbf{q}_n} = 2\mathbf{T}_{CB} \left[ q_w \mathbf{a} + \mathbf{q}_v \times \mathbf{a} \mid \mathbf{q}_v^T \mathbf{a} \mathbf{I}_{3 \times 3} + \mathbf{q}_v \mathbf{a}^T - \mathbf{a} \mathbf{q}_v^T - q_w \left[ \mathbf{a} \right]_{\times} \right] \quad (3.24)$$

The whole derivative by the true state results in a  $3 \times 16$  matrix:

$$\mathbf{P}_{\mathbf{x}_t} = \begin{bmatrix} \frac{\partial \mathbf{p}_c^f}{\partial \mathbf{p}_n^b} & \frac{\partial \mathbf{p}_c^f}{\partial \mathbf{q}_n} & \mathbf{0}_{3 \times 9} \end{bmatrix} \quad (3.25)$$



## Jacobian of the true-state with respect to the error-state

Finally,  $\partial \mathbf{x}_t / \partial \delta \mathbf{x}$  should be determined. All derivatives yield the identity block  $\mathbf{I}_3$ , except for the quaternion. The Jacobian of the true quaternion with respect to the error rotation vector is:

$$\frac{\partial(\delta \mathbf{q} \otimes \mathbf{q})}{\partial \delta \boldsymbol{\theta}} = \mathbf{Q}_{\delta \boldsymbol{\theta}} = \frac{1}{2} [\mathbf{q}]_R \begin{bmatrix} \mathbf{0}^T \\ \mathbf{I}_3 \end{bmatrix} \quad (3.26)$$

Detailed calculations can be found in Appendix B.3, which leads to the Jacobian:

$$\frac{\partial \mathbf{x}_t}{\partial \delta \mathbf{x}} = \mathbf{X}_{\delta x} = \begin{bmatrix} \frac{\partial \mathbf{p}_{n,t}}{\partial \delta \mathbf{p}_n} & \dots & \mathbf{0} \\ \vdots & \ddots & \vdots \\ \mathbf{0} & \dots & \frac{\partial \boldsymbol{\beta}_{\omega,t}}{\partial \delta \boldsymbol{\beta}_\omega} \end{bmatrix} = \begin{bmatrix} \mathbf{I}_3 & \mathbf{0} & \mathbf{0} \\ \mathbf{0} & \mathbf{Q}_{\delta \ominus} & \mathbf{0} \\ \mathbf{0} & \mathbf{0} & \mathbf{I}_9 \end{bmatrix} \quad (3.27)$$

### 3.3.3 Error injection into the nominal-state

After performing an update on the error-state, its mean has to be injected into the nominal-state. All quantities require a simple summary of the nominal- and error- states, except for the rotation which can be performed as a left-side quaternion multiplication by the error quaternion. These operations were provided in Table 3.1, therefore the injection procedure:

$$\mathbf{p}_n = \mathbf{p}_n + \delta \hat{\mathbf{p}}_n \quad (3.28a)$$

$$\mathbf{q}_n = \mathbf{q} \{ \delta \hat{\boldsymbol{\theta}} \} \otimes \mathbf{q}_n \quad (3.28b)$$

$$\mathbf{v}_b = \mathbf{v}_b + \delta \hat{\mathbf{v}}_b \quad (3.28c)$$

$$\boldsymbol{\beta}_a = \boldsymbol{\beta}_a + \delta \hat{\boldsymbol{\beta}}_a \quad (3.28d)$$

$$\boldsymbol{\beta}_\omega = \boldsymbol{\beta}_\omega + \delta \hat{\boldsymbol{\beta}}_\omega \quad (3.28e)$$

Next, the error-state gets reset, therefore its mean has to be removed, which is done by the inverse operations above. I'm denoting this operation with  $\delta \mathbf{x}^+ =$

$g(\delta\mathbf{x}_k)$ , which can be expressed as:

$$\delta\mathbf{p}_n^+ = \delta\mathbf{p}_n - \hat{\delta\mathbf{p}}_n \quad (3.29a)$$

$$\delta\boldsymbol{\theta}^+ = 2 \begin{bmatrix} \mathbf{0} & \mathbf{0}^T \\ \mathbf{0} & \mathbf{I}_3 \end{bmatrix} (\mathbf{q}\{\delta\boldsymbol{\theta}\} \otimes \mathbf{q}\{-\hat{\delta\boldsymbol{\theta}}\}) \quad (3.29b)$$

$$\delta\mathbf{v}_b^+ = \delta\mathbf{v}_b - \hat{\delta\mathbf{v}}_b \quad (3.29c)$$

$$\delta\boldsymbol{\beta}_a^+ = \delta\boldsymbol{\beta}_a - \hat{\delta\boldsymbol{\beta}}_a \quad (3.29d)$$

$$\delta\boldsymbol{\beta}_\omega^+ = \delta\boldsymbol{\beta}_\omega - \hat{\delta\boldsymbol{\beta}}_\omega \quad (3.29e)$$

In fact, the error-state is not directly estimated by the filter, as a result only the mean and the covariance matrix have to be updated. Obviously, the mean resets to zeros, but the covariance matrix update depends on  $g(\cdot)$ , thus the full error reset:

$$\hat{\delta\mathbf{x}} = \mathbf{0} \quad (3.30a)$$

$$\mathbf{P}^+ = \mathbf{G}\mathbf{P}\mathbf{G}^T \quad (3.30b)$$

Here,  $\mathbf{G}$  is the Jacobian matrix of  $g(\cdot)$ , defined as:

$$\mathbf{G} = \left. \frac{\partial g}{\partial \delta\mathbf{x}} \right|_{\hat{\delta\mathbf{x}}} = \begin{bmatrix} \mathbf{I}_3 & \mathbf{0} & \mathbf{0} \\ \mathbf{0} & \mathbf{I} + \left[ \frac{1}{2}\hat{\delta\boldsymbol{\theta}} \right]_{\times} & \mathbf{0} \\ \mathbf{0} & \mathbf{0} & \mathbf{I}_9 \end{bmatrix} \quad (3.31)$$

Similarly to what happened with the update Jacobian before, all quantities result in identity blocks, except the orientation part. The calculations related to the formula above are detailed in Appendix B.4.

# CHAPTER 4

## OVERVIEW OF THE TRIANGULATION

### METHOD

---

In the previous chapter, the ESKF was introduced as a method capable of updating the state using camera measurements, provided that the precise localization coordinates of visible feature points are known. However, in practical applications, assuming prior knowledge of the coordinates of these visible feature points is often untenable. Consequently, there arises the need to estimate these coordinates, a process commonly referred to as triangulation.

This chapter provides an in-depth look at the triangulation method applied in this study, with a focus on its integration into our visual-inertial navigation system. The foundation of this method draws from [19], utilizing the core equations as described therein. However, their approach only takes into account uncertainties in the camera measurements, but our system requires to consider uncertainties in the states too.

The central objective of this chapter is to explain the key components and modifications in the custom-made triangulation approach. In particular, answers will be given to questions such as how position and orientation are involved in the LOST equations, and how can be formed the recursive version of LOST.

#### 4.1 Problem statement

The modern triangulation problem takes on one of two forms: intersection or resection [20], shown in the figure 4.1.

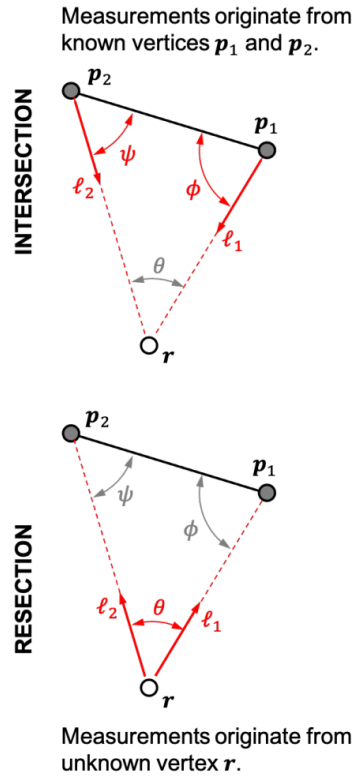


**Figure 4.1:** Illustration of intersection (top) and resection (bottom) forms of the triangulation problem ([19]: page 3)

The main difference between the two formalizations is that the intersection assumes measurements taken from known vertices and the goal is to determine the position of a visible feature point ( $r$ ). On the other hand, the resection problem supposes known visible vertices and aims to estimate the position where the measurement was taken.

The intersection problem has many practical applications such as satellite orbit determination [21, 22], and 3-D scene reconstruction usually called Structure from Motion (SfM) [23, 24, 25]. The resection problem describes the vehicle localization problem that is generally included in navigation applications [13, 14, 26]. In this project, both forms are applied, because LOST is used to optimize 3-D coordinates of visible feature points which basically means a 3-D reconstruction of the environment. On the contrary, the Kalman filter update is the form of a resection problem in the sense that the optimized LOST estimates are used to improve the state estimates.

### 4.1.1 Line of sight (LOS) measurements

The triangulation problem typically involves angles acquired through various optical instruments. In vehicle navigation, angles are often derived from images captured by cameras or telescopes. Regardless of the specific application, the angle measurements obtained through these optical instruments describe the direction from the sensor to the observed point. In other words, they express the path from one vertex of a triangle to another, and this direction represents a straight line connecting these two points, commonly known as the "line of sight" (LOS).

Before I would delve into the details, it's important to establish a few mathematical notation:

- $\begin{bmatrix} u_i & v_i & f \end{bmatrix}^T = \bar{\mathbf{u}}_i = \mathbf{K}\mathbf{u}_i$ , it is worth highlighting that the LOS measurement can be derived from actual measurement using  $\mathbf{u}_i = \mathbf{K}^{-1}\bar{\mathbf{u}}_i$ . However, it is important to emphasize that this transformation accounts for both the adjustment of the principal point and multiplying the vector with the focal length. Later merely introduces a scaling factor, which is inherently resolved in LOST equations.
- $\mathbf{u}_i \propto \mathbf{a}_i \propto \mathbf{p}_{c,i}^f$ , where  $\mathbf{a}_i = \frac{\mathbf{u}_i}{\|\mathbf{u}_i\|} = \frac{\mathbf{p}_{c,i}^f}{\|\mathbf{p}_{c,i}^f\|}$
- $\mathbf{p}_{c,i}^f = \rho\mathbf{a}_i$ , where  $\rho$  denotes the range from the sensor to the observed point

## 4.2 LOST method

When more than 2 LOS measurements are available the polynomial methods do not scale easily, therefore the LOST suggests a Maximum Likelihood Estimation (MLE) solution for an unknown vertex ( $\mathbf{p}_n^f$ ). The linear system can be created by double applications of the Law of Sines which trigonometric law relates the angles and side lengths of a triangle.

The initial equation is the Direct Linear Transform (DLT) form of the Law of Sines. This mathematical prescription removes the unknown scale ambiguity along the LOS trajectory, achieved by utilizing the collinearity of the camera measurement

and feature point position in the camera system:

$$\mathbf{p}_c^f = \mathbf{R}_{CN}(\mathbf{p}_n^f - \mathbf{p}_n^c) = \mathbf{R}_{CB}(\mathbf{R}_{BN}(\mathbf{p}_n^f - \mathbf{p}_n^b) - \mathbf{p}_b^c) \quad (4.1)$$

$$\left[ \mathbf{u}_i \right]_{\times} \mathbf{p}_c^f = \left[ \mathbf{u}_i \right]_{\times} \mathbf{R}_{CB}(\mathbf{R}_{BN}(\mathbf{p}_n^f - \mathbf{p}_n^b) - \mathbf{p}_b^c) = \mathbf{0} \quad (4.2)$$

### 4.2.1 Covariance calculations

(4.2) is only true if every value is ideal. When only the noisy measurements and nominal states are available, the right-hand side is no longer exactly zero:

$$\left[ \mathbf{u}_i \right]_{\times} \mathbf{p}_c^f = \boldsymbol{\epsilon}_i \quad (4.3)$$

$\boldsymbol{\epsilon}_i$  can be calculated by applying the previously introduced error models which are just an additional error in the case of body position and measurement noise, but the Taylor series approximation for the rotation. Using the notation  $\mathbf{u}_t = \mathbf{u} + \delta\mathbf{u}$  for the measurement model, the cross-product results in:

$$\boldsymbol{\epsilon}_i = \left[ \mathbf{u}_i \right]_{\times} \mathbf{R}_{CN} \delta \mathbf{p}_n^b + \left[ \mathbf{u}_i \right]_{\times} \left[ \rho \mathbf{a}_i + \mathbf{T}_{CB} \mathbf{p}_b^c \right]_{\times} \mathbf{T}_{CB} \delta \boldsymbol{\theta} + \rho \left[ \mathbf{a}_i \right]_{\times} \delta \mathbf{u}_i \quad (4.4)$$

In (4.4) there was used the property  $\rho \mathbf{a}_i = \mathbf{p}_c^f$ , because  $\mathbf{p}_c^f$  is not known apriori, but the scaling factor can be calculated with applying the Law of Sines. Let's consider the intersection problem in Figure 4.1, the traveled distance can be determined as  $\mathbf{d}_{ij} = \mathbf{p}_{n,j}^c - \mathbf{p}_{n,i}^c = \mathbf{p}_{n,j}^b - \mathbf{p}_{n,i}^b$ , and applying law of sines on vertex  $\mathbf{p}_{n,j}^b$  and  $\mathbf{p}_n^f$ :

$$\frac{\|\mathbf{p}_{c,j}^f\|}{\sin \phi} = \frac{\|\mathbf{d}_{ij}\|}{\sin \theta} \Rightarrow \rho_j = \|\mathbf{p}_{c,j}^f\| = \frac{\|\mathbf{d}_{ij}\| \sin \phi}{\sin \theta} = \frac{\|\mathbf{d}_{ij} \times \mathbf{a}_i\|}{\|\mathbf{a}_i \times \mathbf{a}_j\|}, \quad (4.5)$$

where the DLT form of the law of sines was given. Note that the formula above is only valid in consistent frames.

Utilizing the position and orientation covariance and cross-covariance matrices from the filter or GPS measurements and assuming no correlation between them and the measurement noise ( $\mathbf{V}$ ), then the covariance of  $\epsilon_i$  is calculated as:

$$\begin{aligned} \mathbf{T} &= \left[ \begin{array}{cc} \left[ \mathbf{u}_i \right]_{\times} \mathbf{R}_{CN} & \left[ \mathbf{u}_i \right]_{\times} \left[ \rho \mathbf{a}_i + \mathbf{T}_{CB} \mathbf{p}_b^c \right]_{\times} \mathbf{T}_{CB} \\ \rho \left[ \mathbf{a}_i \right]_{\times} & \end{array} \right], \\ \mathbf{P}_{\epsilon_i} &= E\{\epsilon_i \epsilon_i^T\} = \mathbf{T} \begin{bmatrix} \mathbf{P}_{\delta p_n^b, \delta \theta} & \mathbf{0}_{6 \times 3} \\ \mathbf{0}_{3 \times 6} & \mathbf{V} \end{bmatrix} \mathbf{T}^T \end{aligned} \quad (4.6)$$

## 4.2.2 The optimal solution

One may write the MLE problem to minimize  $\epsilon$  by variable  $\mathbf{p}_n^f$ :

$$\min J(\mathbf{p}_n^f) = \sum_{i=1}^n \epsilon_i^T \mathbf{P}_{\epsilon_i}^{-1} \epsilon_i \quad (4.7)$$

Since  $\mathbf{P}_{\epsilon_i}$  is always rank deficient due to skew-matrices involved in its calculation and also the pixel error is only 2-D, henceforth the approximation  $\mathbf{P}_{\epsilon_i}^{-1} \rightarrow \mathbf{P}_{\epsilon_i}^+$  will be used, where  $+$  denotes the Moore-Penrose inverse. After a short detour, I return to (4.7) which after substituting (4.4) and considering only terms consisting  $\mathbf{p}_n^f$ :

$$\begin{aligned} \min J(\mathbf{p}_n^f) &= \mathbf{p}_n^{fT} \sum_{i=1}^n \mathbf{R}_{NC,i} \left[ \mathbf{u}_i \right]_{\times} \mathbf{P}_{\epsilon_i}^+ \left[ \mathbf{u}_i \right]_{\times} \mathbf{R}_{CB} (\mathbf{R}_{BN,i} \mathbf{p}_{n,i}^b + \mathbf{p}_b^c) \\ &\quad + \left( \sum_{i=1}^n (\mathbf{R}_{BN,i} \mathbf{p}_{n,i}^b + \mathbf{p}_b^c)^T \mathbf{R}_{BC} \left[ \mathbf{u}_i \right]_{\times} \mathbf{P}_{\epsilon_i}^+ \left[ \mathbf{u}_i \right]_{\times} \mathbf{R}_{CN,i} \right) \mathbf{p}_n^f \\ &\quad - \mathbf{p}_n^{fT} \left( \sum_{i=1}^n \mathbf{R}_{NC,i} \mathbf{P}_{\epsilon_i}^+ \mathbf{R}_{CN,i} \right) \mathbf{p}_n^f \end{aligned} \quad (4.8)$$

Applying the 1<sup>st</sup> differential condition on (4.8):

$$\begin{aligned} \frac{\partial \min J(\mathbf{p}_n^f)}{\partial \mathbf{p}_n^f} &= \\ &= -2 \sum_{i=1}^n \mathbf{R}_{NC,i} \left[ \mathbf{u}_i \right]_{\times} \mathbf{P}_{\epsilon_i}^+ \left[ \mathbf{u}_i \right]_{\times} \mathbf{R}_{CB} (\mathbf{R}_{BN,i} (\mathbf{p}_n^f - \mathbf{p}_{n,i}^b) - \mathbf{p}_b^c) = 0 \end{aligned} \quad (4.9)$$

Rearranging the terms the linear equation system which has to be solved is:

$$\left( \sum_{i=1}^n \mathbf{R}_{NC,i} [\mathbf{u}_i]_{\times} \mathbf{P}_{\epsilon_i}^+ [\mathbf{u}_i]_{\times} \mathbf{R}_{CN,i} \right) \mathbf{p}_n^f = \sum_{i=0}^n \mathbf{R}_{NC,i} [\mathbf{u}_i]_{\times} \mathbf{P}_{\epsilon_i}^+ [\mathbf{u}_i]_{\times} \mathbf{R}_{CB} (\mathbf{R}_{BN,i} \mathbf{p}_{n,i}^b + \mathbf{p}_b^c) \quad (4.10)$$

### 4.2.3 Practical formalization of the estimator

The usual approach for solving least squares systems is to avoid the explicit formation of the normal equations, and instead solve (4.10) with an alternative technique such as solving it through factorization [27].

Since the weighting matrix  $\mathbf{P}_{\epsilon_i}^+$  is calculated from a covariance matrix which is positive semi-definite, therefore it has real non-negative eigenvalues and real eigenvectors. With the help of eigendecomposition,  $\mathbf{P}_{\epsilon_i}^+$  can be factorized as  $\mathbf{P}_{\epsilon_i}^+ = \mathbf{V}_i \mathbf{D}_i \mathbf{V}_i^T = (\mathbf{V}_i \sqrt{\mathbf{D}_i})(\mathbf{V}_i \sqrt{\mathbf{D}_i})^T = \mathbf{B}_i \mathbf{B}_i^T$ .

Decomposing (4.10) with notation  $\mathbf{A}_i = \mathbf{B}_i^T [\mathbf{u}_i]_{\times} \mathbf{R}_{CN,i}$  it yields:

$$\overbrace{\begin{bmatrix} \mathbf{A}_1 \\ \vdots \\ \mathbf{A}_n \end{bmatrix}}^{\mathbf{A}} \mathbf{p}_n^f = \overbrace{\begin{bmatrix} \mathbf{A}_1 (\mathbf{p}_{n,1}^b + \mathbf{R}_{NB,1} \mathbf{p}_b^c) \\ \vdots \\ \mathbf{A}_n (\mathbf{p}_{n,n}^b + \mathbf{R}_{NB,n} \mathbf{p}_b^c) \end{bmatrix}}^{\mathbf{b}} \quad (4.11)$$

The above equation must be solved in least squares terms, which means the estimator is calculated as:

$$\hat{\mathbf{p}}_n^f = \mathbf{A}^+ \mathbf{b} \quad (4.12)$$

### 4.2.4 Covariance of the estimator

As a result of statistically optimal weighting the estimator covariance can be computed as:



$$\mathbf{P}_{p_n^f} = \left( \sum_{i=1}^n \mathbf{A}_i^T \mathbf{A}_i \right)^{-1} \quad (4.13)$$

It is worth to mention that  $\mathbf{A}_i^T \mathbf{A}_i$  matrices are rank deficient, therefore the inverse calculation accuracy can degrade especially when the number of samples is low, thus the application of pseudoinverse is recommended.

### 4.3 The recursive version

An additional advantage of decomposing the linear system is that the estimator takes the form of a general LS solution, for which the recursive version is easy to find. Initially, let's formalize the estimation until the  $i^{th}$  estimation based on (4.12):

$$\hat{\mathbf{p}}_{n,i}^f = \left( \sum_i \mathbf{A}_i^T \mathbf{A}_i \right)^{-1} \left( \sum_i \mathbf{A}_i^T \mathbf{y}_i \right) = \mathbf{P}_{p_{n,i}^f} \mathbf{b}_i, \quad (4.14)$$

note that  $\mathbf{b}_i = \mathbf{P}_{p_{n,i}^f}^{-1} \hat{\mathbf{p}}_{n,i}^f$ . Then the  $(i+1)^{th}$  estimation is:

$$\begin{aligned} \hat{\mathbf{p}}_{n,i+1}^f &= \mathbf{P}_{p_{n,i+1}^f} \left( \mathbf{b}_i + \mathbf{A}_{i+1}^T \mathbf{y}_{i+1} \right) \\ &= \mathbf{P}_{p_{n,i+1}^f} \left( \mathbf{P}_{p_{n,i}^f}^{-1} \hat{\mathbf{p}}_{n,i}^f + \mathbf{A}_{i+1}^T \mathbf{y}_{i+1} \right) \\ &= \mathbf{P}_{p_{n,i+1}^f} \left( \left( \mathbf{P}_{p_{n,i+1}^f}^{-1} - \mathbf{A}_{i+1}^T \mathbf{A}_{i+1} \right) \hat{\mathbf{p}}_{n,i}^f + \mathbf{A}_{i+1}^T \mathbf{y}_{i+1} \right) \\ &= \hat{\mathbf{p}}_{n,i}^f + \mathbf{P}_{p_{n,i+1}^f} \mathbf{A}_{i+1}^T \left( \mathbf{y}_{i+1} - \mathbf{A}_{i+1} \hat{\mathbf{p}}_{n,i}^f \right), \end{aligned} \quad (4.15)$$

where  $\mathbf{A}_{i+1}$  and  $\mathbf{y}_{i+1}$  can be calculated from new data, and the covariance matrix can be propagated based on (4.13):

$$\mathbf{P}_{p_{n,i+1}^f} = \left( \left( \mathbf{P}_{p_{n,i}^f} \right)^{-1} + \mathbf{A}_{i+1}^T \mathbf{A}_{i+1} \right)^{-1} \quad (4.16)$$

# CHAPTER 5

## SYNERGIZING LOST AND ESKF

### FOR ROBUST NAVIGATION

---

In the previous two chapters, the applied filter technique and triangulation approach were introduced, and now the focus shifts toward the integration of the two methods. This integration process will begin by examining the impact on the Kalman gain, a crucial component in the navigation system. Furthermore, the discussion extends to the role of cross-covariances in the process of integration.

#### 5.1 The modified Kalman gain

The derivation of the Kalman gain is based on [28], but adopted to the implemented system. Firstly, the integration affects the Kalman gain because forming the residual involves both the triangulated feature position and the filter state. Previously, only the uncertainty of the state was assumed, but as soon as the true values of the 3-D feature position are not known, then its uncertainty should be taken into account too.

The derivation of the new Kalman gain requires looking into the prediction step of the ESKF because compared to a conventional Kalman filter, the ESKF has multiple prediction steps between two updates. The true value of the error-state is given by (3.17) and the predicted error-state by (3.18b), extending them for N prediction it yields:

$$\begin{aligned}\delta\mathbf{x}_{k+N} &= \left( \prod_{j=0}^{N-1} \mathbf{F}_{x,k+j} \right) \delta\mathbf{x}_k + \left[ \sum_{j=0}^{N-1} \left( \prod_{l=j+1}^{N-1} \mathbf{F}_{x,k+l} \right) \mathbf{F}_{i,k+j} \mathbf{i}_{k+j} \right] \\ &= \mathbf{P}\mathbf{F}_x^N \delta\mathbf{x}_k + \mathbf{S}\mathbf{F}_i^N \mathbf{i}\end{aligned}\tag{5.1a}$$

$$\delta\hat{\mathbf{x}}_{k+N}^- = \left( \prod_{j=0}^{N-1} \mathbf{F}_{x,k+j} \right) \delta\hat{\mathbf{x}}_k = \mathbf{PF}_x^N \delta\hat{\mathbf{x}}_k, \quad (5.1b)$$

where the - superscript denotes that these states are the result of the forecast alias prediction step. Next, using the above formulas the linearized actual and the estimated measurements can be written as:

$$\mathbf{z}_{k+N} \approx h(\mathbf{x}_{k+N}, \mathbf{p}_{n,k}^f) + \mathbf{H}_{x,k+N} \delta\mathbf{x}_{k+N} + \mathbf{H}_{f,k+N} \delta\mathbf{p}_{n,k}^f + \delta\mathbf{u}_{k+N} \quad (5.2a)$$

$$\hat{\mathbf{z}}_{k+N} \approx h(\mathbf{x}_{k+N}, \mathbf{p}_{n,k}^f) + \mathbf{H}_{x,k+N} \delta\hat{\mathbf{x}}_{k+N}^- + \mathbf{H}_{f,k+N} \delta\hat{\mathbf{p}}_{n,k}^f \quad (5.2b)$$

After the measurement update, the new a posteriori estimation is:

$$\begin{aligned} \delta\hat{\mathbf{x}}_{k+N} &= \delta\hat{\mathbf{x}}_{k+N}^- + \mathbf{K}(\mathbf{z}_{k+N} - \hat{\mathbf{z}}_{k+N}) \\ &= \delta\hat{\mathbf{x}}_{k+N}^- + \mathbf{K}(\mathbf{H}_{x,k+N} \delta\tilde{\mathbf{x}}_{k+N} + \mathbf{H}_{f,k+N} \delta\tilde{\mathbf{p}}_{n,k}^f + \delta\mathbf{u}_{k+N}), \end{aligned} \quad (5.3)$$

where  $\delta\tilde{\mathbf{x}}_{k+N} = \delta\mathbf{x}_{k+N} - \delta\hat{\mathbf{x}}_{k+N}^-$  and  $\delta\tilde{\mathbf{p}}_{n,k}^f = \delta\mathbf{p}_{n,k}^f - \delta\hat{\mathbf{p}}_{n,k}^f$  were considered as the error of estimations. Then the error of the estimation can be expressed:

$$\begin{aligned} \mathbf{e}_{k+N} &= \delta\mathbf{x}_{k+N} - \delta\hat{\mathbf{x}}_{k+N} = \mathbf{PF}_x^N (\delta\mathbf{x}_k - \delta\hat{\mathbf{x}}_k) + \mathbf{SF}_i^N \mathbf{i} \\ &\quad - \mathbf{K}(\mathbf{H}_{x,k+N} \delta\tilde{\mathbf{x}}_{k+N} + \mathbf{H}_{p,k+N} \delta\tilde{\mathbf{p}}_{n,k}^f + \delta\mathbf{u}_{k+N}) \end{aligned} \quad (5.4)$$

Substituting  $\delta\tilde{\mathbf{x}}_{k+N}$  into the above equation, utilizing  $\mathbf{e}_k = \delta\mathbf{x}_k - \delta\hat{\mathbf{x}}_k$  and collecting the terms leads to the a posteriori error:

$$\mathbf{e}_{k+N} = \overbrace{(\mathbf{I} - \mathbf{KH}_{x,k+N})}^{\mathbf{T}_x} \left( \mathbf{PF}_x^N \mathbf{e}_k + \mathbf{SF}_i^N \mathbf{i} \right) - \overbrace{\mathbf{KH}_{p,k+N}}^{\mathbf{T}_f} \delta\tilde{\mathbf{p}}_{n,k}^f - \mathbf{K} \delta\mathbf{u}_{k+N} \quad (5.5)$$

In order to give an optimal solution for the Kalman gain the a posteriori covariance should be expressed, but this requires some considerations. The first is that our approach updates the state first, then optimizes the feature coordinates with the same measurements which leads to correlation between  $\mathbf{e}_k$  and  $\delta\tilde{\mathbf{p}}_{n,k}^f$ . The other is that in the above equation, the true error state appeared which covariance is calculated by (3.18c) and here the result of this equation will be denoted

as  $\mathbf{P}_{k+N}^-$ . Then the a posteriori covariance is:

$$\begin{aligned}
\mathbf{P}_{k+N} &= E\{\mathbf{e}_{k+N}\mathbf{e}_{k+N}^T\} \\
&= \mathbf{T}_x \mathbf{P}_{k+N}^- \mathbf{T}_x^T + \mathbf{T}_f \overbrace{E\{\delta\tilde{\mathbf{p}}_{n,k}^f (\delta\tilde{\mathbf{p}}_{n,k}^f)^T\}}^{\mathbf{P}_k^f} \mathbf{T}_f^T + \mathbf{K} \underbrace{E\{\delta\mathbf{u}_{k+N}\delta\mathbf{u}_{k+N}^T\}}_{\mathbf{V}} \mathbf{K}^T \\
&\quad - \mathbf{T}_x \underbrace{\mathbf{P}\mathbf{F}_x}_{\mathbf{P}_k^{xf}} E\{\mathbf{e}_k (\delta\tilde{\mathbf{p}}_{n,k}^f)^T\} \mathbf{T}_f^T - \mathbf{T}_f \underbrace{E\{\delta\tilde{\mathbf{p}}_{n,k}^f \mathbf{e}_k^T\}}_{\mathbf{P}_k^{fx}} (\mathbf{P}\mathbf{F}_x)^T \mathbf{T}_x^T
\end{aligned} \tag{5.6}$$

Now, in the last steps, only an optimal Kalman gain should be calculated, in the sense that it minimizes the trace of the posterior covariance. For starters, let's formalize the a posteriori covariance by extracting the terms containing  $\mathbf{K}$ :

$$\begin{aligned}
\mathbf{P}_{k+N} &= \mathbf{P}_{k+N}^- - \mathbf{K} \left( \mathbf{H}_{x,k+N} \mathbf{P}_{k+N}^- + \mathbf{H}_{f,k+N} \mathbf{P}_k^{fx} (\mathbf{P}\mathbf{F}_x)^T \right) \\
&\quad - \left( \mathbf{P}_{k+N}^- \mathbf{H}_{x,k+N}^T + \mathbf{P}\mathbf{F}_x \mathbf{P}_k^{fx} \mathbf{H}_{f,k+N}^T \right) \mathbf{K}^T \\
&\quad + \mathbf{K} \left( \mathbf{H}_{x,k+N} \mathbf{P}_{k+N}^- \mathbf{H}_{x,k+N}^T + \mathbf{H}_{f,k+N} \mathbf{P}_k^f \mathbf{H}_{f,k+N}^T + \mathbf{V} \right. \\
&\quad \left. + \mathbf{H}_{x,k+N} \mathbf{P}\mathbf{F}_x \mathbf{P}_k^{xf} + \mathbf{H}_{f,k+N} \mathbf{P}_k^f \mathbf{F}_x (\mathbf{P}\mathbf{F}_x)^T \mathbf{H}_{x,k+N}^T \right) \mathbf{K}^T
\end{aligned} \tag{5.7}$$

Finally, the optimal Kalman gain can be computed from the above equation:

$$\begin{aligned}
\mathbf{K} &= \frac{\partial \text{tr}(\mathbf{P}_{k+N})}{\partial \mathbf{K}} = \left( \mathbf{P}_{k+N}^- \mathbf{H}_{x,k+N}^T + \mathbf{P}\mathbf{F}_x \mathbf{P}_k^{fx} \mathbf{H}_{f,k+N}^T \right) \\
&\quad \left( \mathbf{H}_{x,k+N} \mathbf{P}_{k+N}^- \mathbf{H}_{x,k+N}^T + \mathbf{H}_{f,k+N} \mathbf{P}_k^f \mathbf{H}_{f,k+N}^T + \mathbf{V} \right. \\
&\quad \left. + \mathbf{H}_{x,k+N} \mathbf{P}\mathbf{F}_x \mathbf{P}_k^{xf} + \mathbf{H}_{f,k+N} \mathbf{P}_k^f \mathbf{F}_x (\mathbf{P}\mathbf{F}_x)^T \mathbf{H}_{x,k+N}^T \right)^{-1}
\end{aligned} \tag{5.8}$$

## 5.2 Cross-covariance estimation

First of all, I would like to make it clear currently the development is not there to account for correlated errors and to enable full integration of the two methods, although, there are a few ideas that can be a future solution and the objective of this section is to introduce them.

One of them is introduced in [29], called Gaussian cosimulation which utilizes the positive semi-definite property of covariance matrices and decomposes them as:

$$\mathbf{P}_1 = E\{\mathbf{y}_1\mathbf{y}_1^T\} = \mathbf{L}_1\mathbf{L}_1^T \quad \mathbf{P}_2 = E\{\mathbf{y}_2\mathbf{y}_2^T\} = \mathbf{L}_2\mathbf{L}_2^T \quad (5.9)$$

Afterward, the method introduces a tuneable parameter  $\rho$  and creates the covariance matrix as:

$$E\{\mathbf{y}_1\mathbf{y}_2^T\} = \rho\mathbf{L}_1\mathbf{L}_2^T \quad (5.10)$$

Since the covariance of the 3-D coordinates of the feature point and the state are not the same dimension, it raises further questions about how can be this method used to generate cross-covariances into the filter update.

# CHAPTER 6

## DEVELOPMENT

---

The initial simulation was developed by SZTAKI System Control Laboratory (SCL) using Matlab/Simulink under the R2019b version, which formed the foundation for subsequent development. The simulation incorporates various toolboxes, including aerospace, UAV, navigation, and real-time Simulink, among others, to enhance its realism. The aircraft model utilizes the parameters of Sindy<sup>1</sup>, while the environment is represented using the WGS84 convention.

During the development, I had to integrate a filter into the simulation, which is mainly based on a user-defined Matlab function block. This block gets the true-state of the aircraft as input and uses this data to project feature points on a camera screen. It also runs an ESKF at 50 Hz, which performs a measurement update after every 10<sup>th</sup> prediction meaning 5 Hz update rate. The results which will be presented are created with simulated noises. The noises are assumed to be isotropic Gaussian white noise, which means their distribution is  $\mathcal{N}(0, \sigma\mathbf{I})$ . The exact dispersion parameters are presented in Table 6.1.

Name	Notation	Value	UoM
Angular velocity measurement noise	$\sigma_{\eta_{\omega}}$	1	$\frac{\circ}{s}$
Acceleration measurement noise	$\sigma_{\eta_a}$	0.1	$\frac{m}{s^2}$
Accelerometer bias noise	$\sigma_{\eta_{\beta a}}$	5	$\frac{mg}{\sqrt{Hz}}$
Gyroscope bias noise	$\sigma_{\eta_{\beta \omega}}$	100	$\frac{\circ}{h\sqrt{Hz}}$

**Table 6.1:** Noise summary

### 6.1 Camera configuration

In the real-world realization, a Basler camera will be used, therefore its parameters were used to configure camera projection. The focal length is 1177.5 px, and

---

<sup>1</sup><http://uav.sztaki.hu/sindy/home.html>

the size of the image is  $2048 \times 1536$  px. The principal point is the image's center, thus  $P_x=1024$  px,  $P_y=768$  px.

During the simulation, I placed a huge amount of feature points on the  $Z=0$  plane of the NED system, which is under the flight path. The angle of the camera ( $\beta$ ) is  $-45^\circ$ , therefore most of the time a lot of feature points are visible in the camera image.

Based on [30], the best practice is to choose feature points equally from each side of the image, because the feature points move mostly at the edges of the image. To sum up, the current solution selects the first 19 visible feature points in a band from the left, right, bottom, and top edges of the image and uses only those that are sufficiently converged. The width of the edges is configurable, an example from the simulation can be seen in Figure 6.1 with 200 px width.

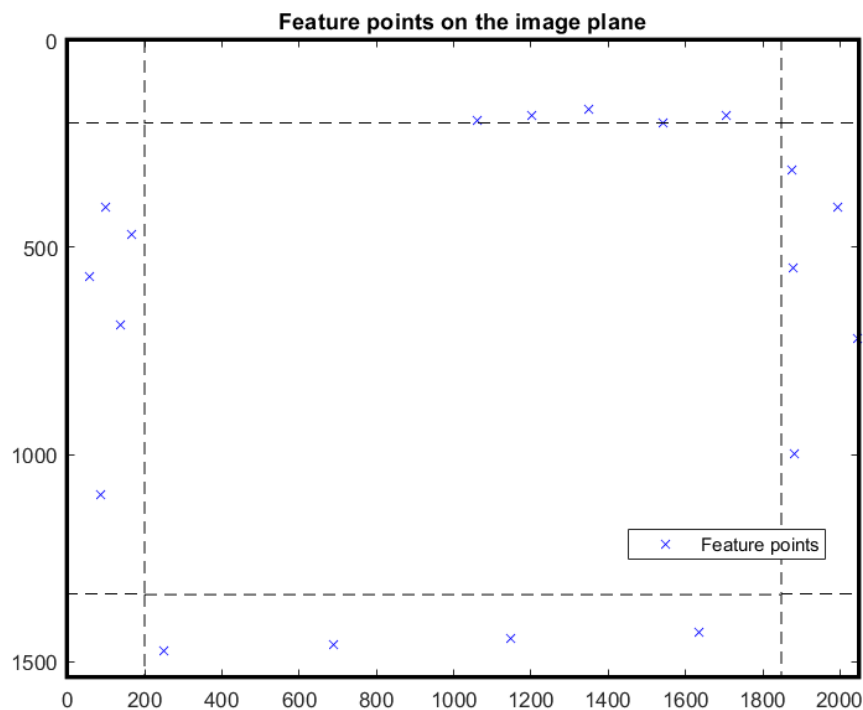


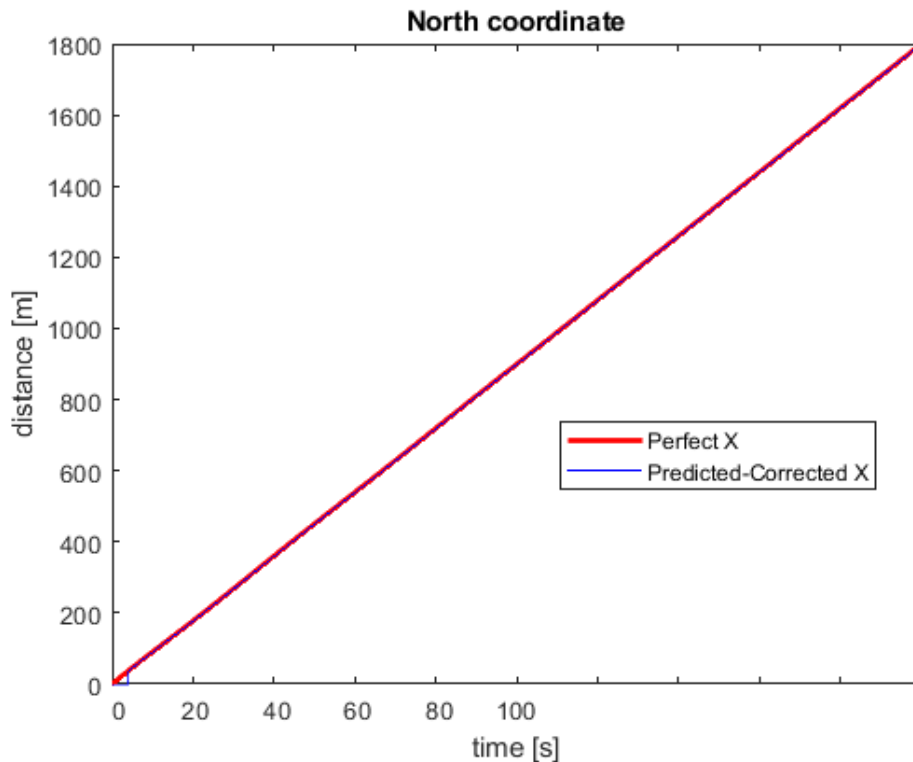
**Figure 6.1:** Camera image example

## 6.2 Simulation setup

The development was done in successive steps, hence the steps:

1. Without any perturbation and update step the filter just integrated the nominal values through time, this validated the correct nominal equations.
2. In the next step, I added process and measurement noises to the system, and the updates were performed by the true value of feature coordinates.
3. Next, I also added biases to the system but still used the perfect values of feature positions.
4. After validating the correct functioning of the filter, I checked the performance of the triangulation method with the usage of true-state values.
5. Finally, the last step is ready a version of the filter, when the LOST estimations were integrated into the filter update, but the LOST used GPS values as input for triangulation.

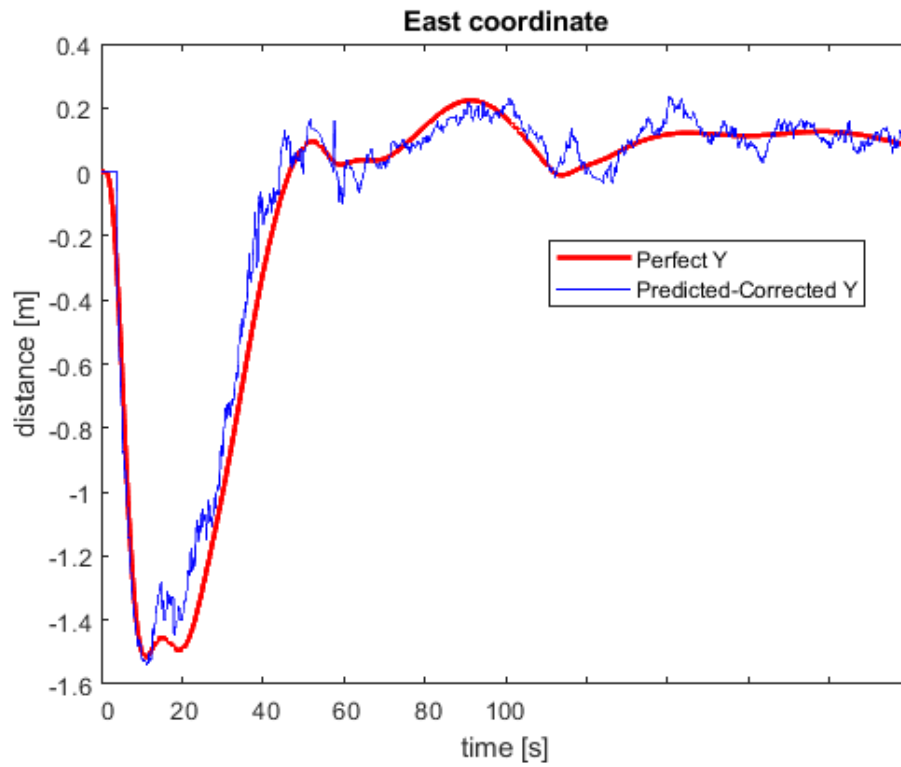
I present the results of the (5) step, where the filter was started at 2s.



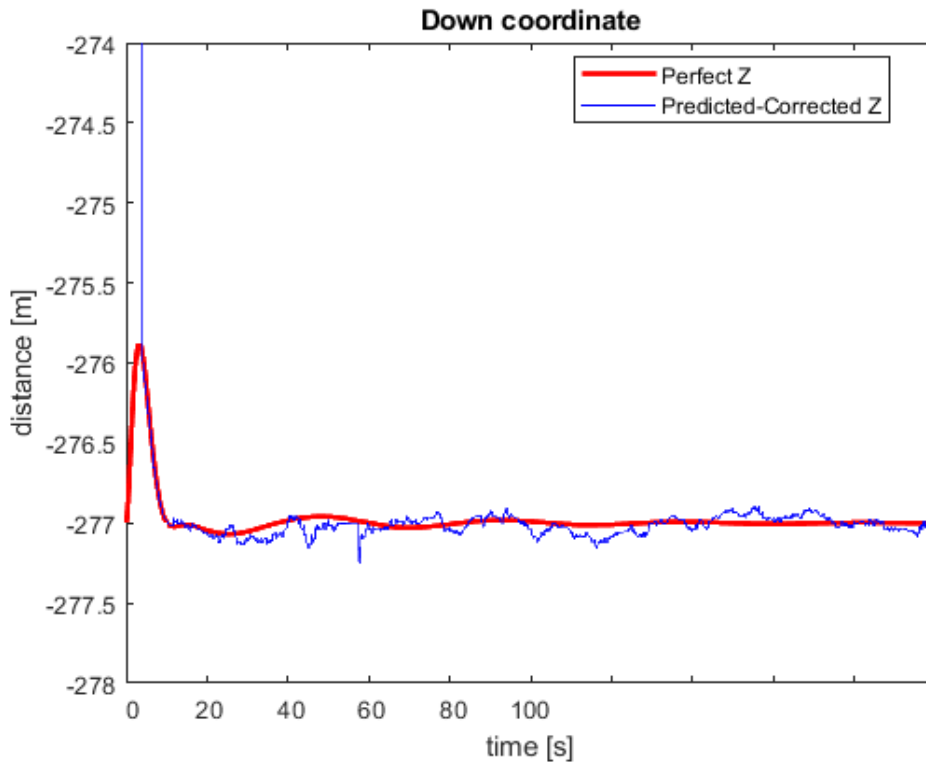
(a) North

**Figure 6.2:** NED coordinates



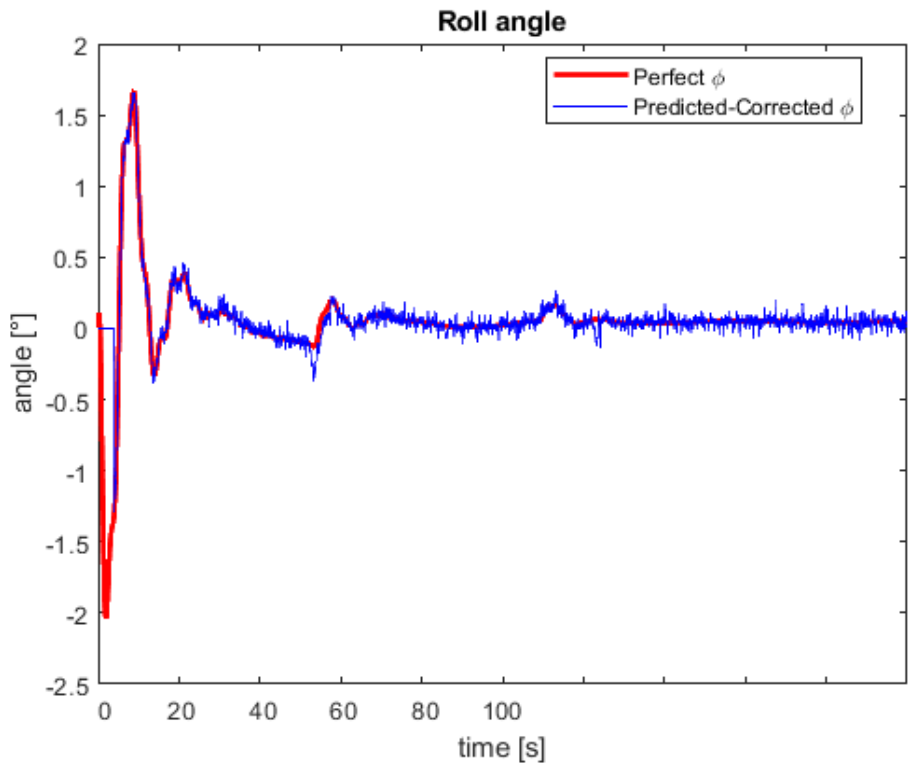


(b) East

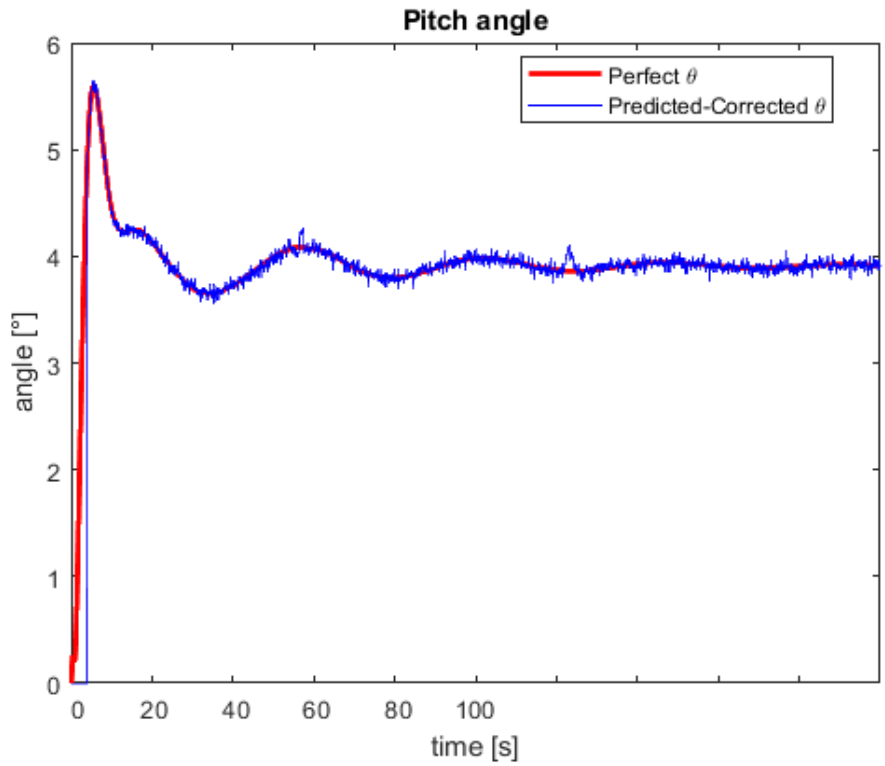


(c) Down

Figure 6.2: NED coordinates (Continued)

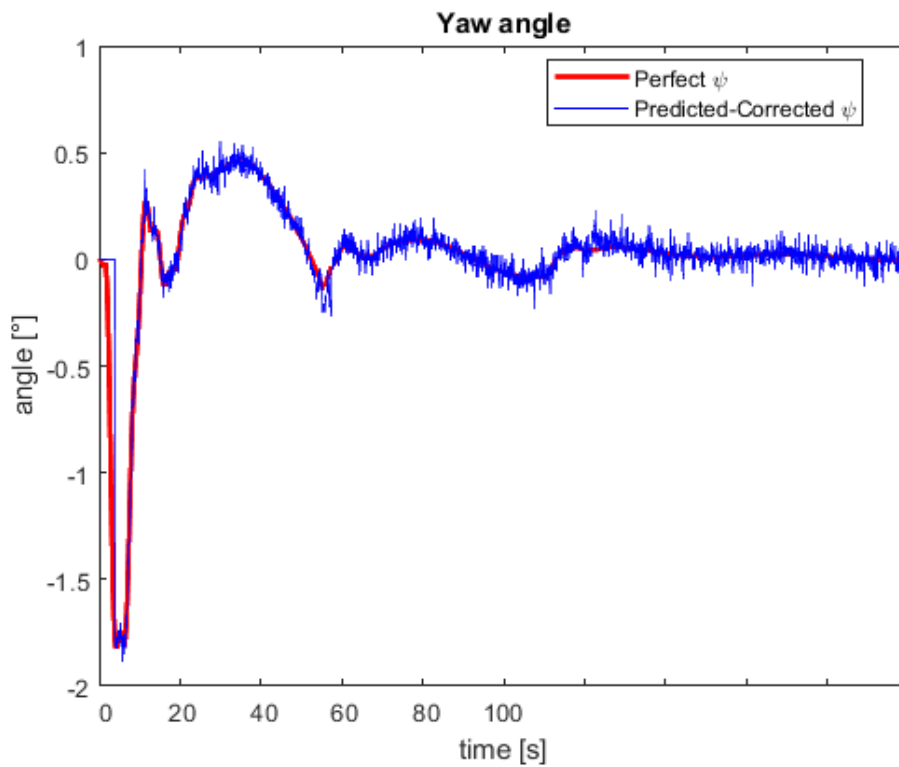


(a) Roll



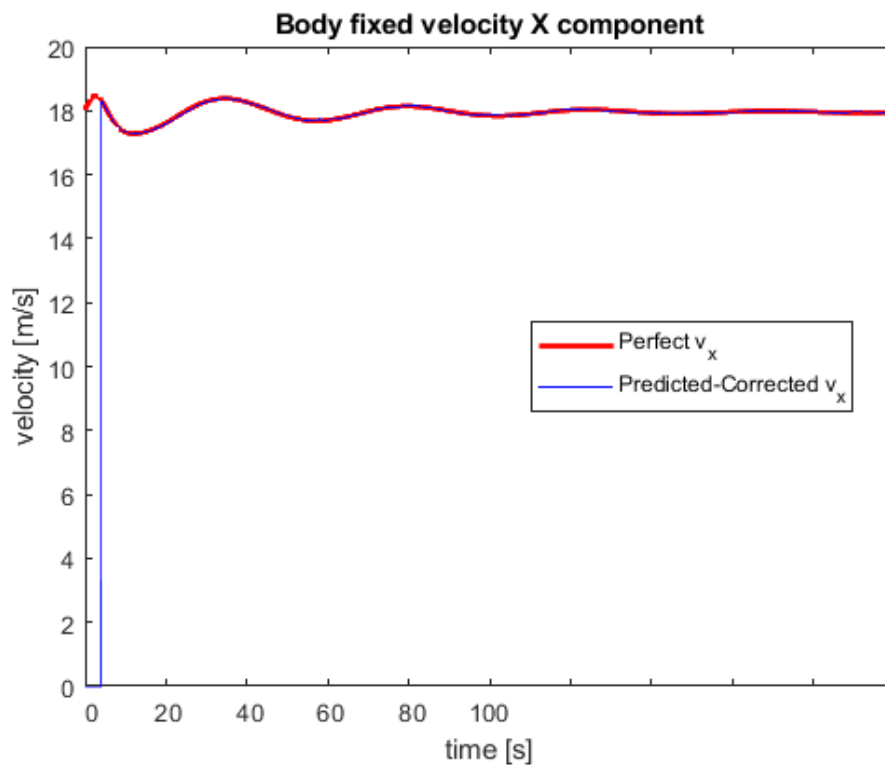
(b) Pitch

Figure 6.3: Euler angles



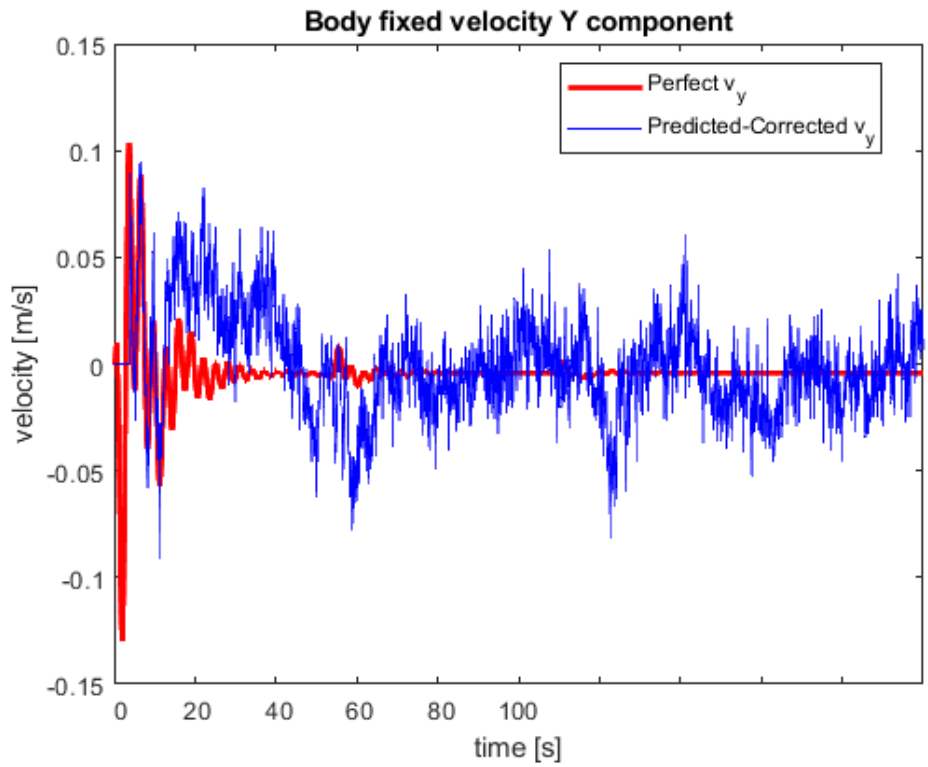
(c) Yaw

Figure 6.3: Euler angles (Continued)

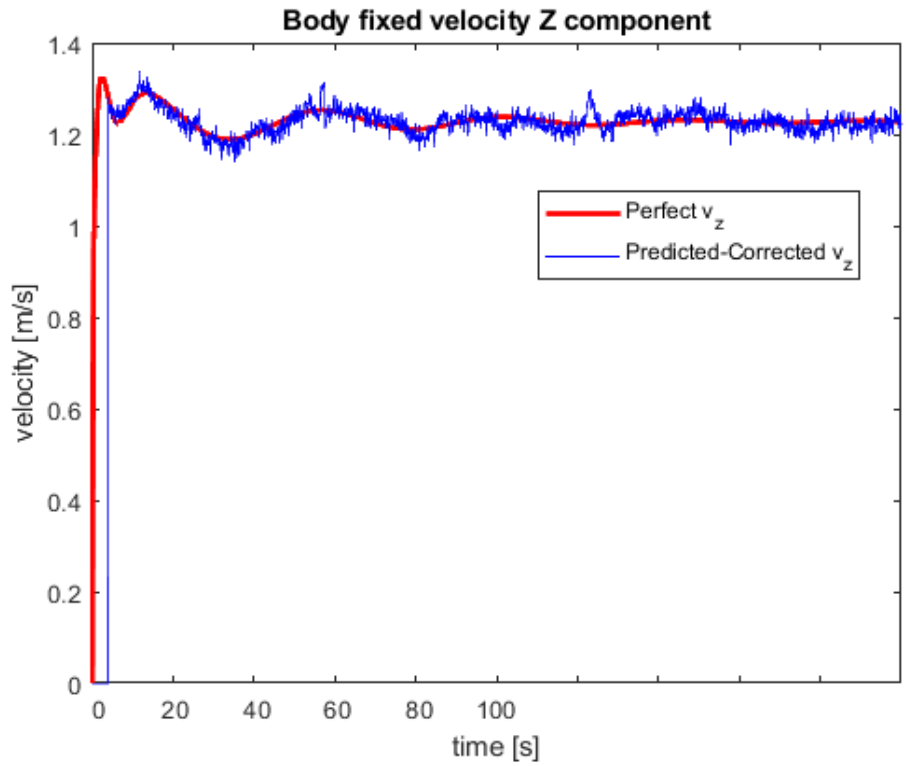


(a) X component

Figure 6.4: Body-fixed velocity



(b) Y component



(c) Z component

**Figure 6.4:** Body-fixed velocity (Continued)

# CHAPTER 7

## CONCLUSION

---

In summary, the integration of ESKF and LOST with assuming known GPS coordinates in the triangulation method can be regarded as a success. However, further advancements are necessary to ensure its practical viability in real-world scenarios. These enhancements encompass the following:

1. Creating a useful cross-covariance estimator method and integrating it into the filter framework.
2. The integration of genuine image processing algorithms into the ESKF framework, leading to:
  - (a) The incorporation of camera imperfections, such as lens distortion errors into the simulation.
  - (b) The enhancement of the measurement update process to rely not solely on a single camera image but also on track information pertaining to feature points.
3. The development of a back-end component for the filter.

# APPENDIX A

## QUATERNION OPERATIONS

---

All of the following formulas can be found in [18].

The Hamiltonian-quaternion multiplication ( $\otimes$ ) is defined as:

$$\mathbf{q} \otimes \mathbf{p} \triangleq \begin{bmatrix} p_w q_w - p_x q_x - p_y q_y - p_z q_z \\ p_w q_x + p_x q_w + p_y q_z - p_z q_y \\ p_w q_y - p_x q_z + p_y q_w + p_z q_x \\ p_w q_z + p_x q_y - p_y q_x + p_z q_w \end{bmatrix} = \begin{bmatrix} p_w q_w - \mathbf{p}_v^T \mathbf{q}_v \\ p_w \mathbf{q}_v + q_w \mathbf{p}_v + \mathbf{p}_v \times \mathbf{q}_v \end{bmatrix} \quad (\text{A.1})$$

The conjugate of a  $\mathbf{q}$  quaternion is defined as:

$$\mathbf{q}^* \triangleq q_w - \mathbf{q}_v = \begin{bmatrix} q_w \\ -\mathbf{q}_v \end{bmatrix} \quad (\text{A.2})$$

The inverse of  $\mathbf{q}$  quaternion is defined as:

$$\mathbf{q}^{-1} = \frac{\mathbf{q}^*}{\|\mathbf{q}\|^2} \Rightarrow \forall \mathbf{q}, (\|\mathbf{q}\| = 1) \rightarrow \mathbf{q}^* = \mathbf{q}^{-1}, \quad (\text{A.3})$$

where the equivalence of the conjugate and the inverse of unit quaternions is similar to the unitary property of the rotation matrices, which leads to the equivalence of the transpose and inverse matrix.

The next important property of quaternions is that the quaternion product can be expressed in matrix form:

$$\mathbf{q}_1 \otimes \mathbf{q}_2 = \begin{bmatrix} \mathbf{q}_1 \end{bmatrix}_L \mathbf{q}_2 \iff \mathbf{q}_1 \otimes \mathbf{q}_2 = \begin{bmatrix} \mathbf{q}_2 \end{bmatrix}_R \mathbf{q}_1, \quad (\text{A.4})$$

where  $[\mathbf{q}_1]_L$  and  $[\mathbf{q}_2]_R$  are the left- and right- quaternion-product matrices, which can be derived from (A.1) and (A.4):

$$[\mathbf{q}]_L = q_w \mathbf{I}_{4 \times 4} + \begin{bmatrix} 0 & -\mathbf{q}_v^T \\ \mathbf{q}_v & [\mathbf{q}_v]_{\times} \end{bmatrix}, \quad [\mathbf{q}]_R = q_w \mathbf{I}_{4 \times 4} + \begin{bmatrix} 0 & -\mathbf{q}_v^T \\ \mathbf{q}_v & -[\mathbf{q}_v]_{\times} \end{bmatrix} \quad (\text{A.5})$$

The relation between quaternions and rotation matrices can be derived from (2.10), (A.4), and (A.5):

$$\begin{bmatrix} 0 \\ \mathbf{v}' \end{bmatrix} = \mathbf{q} \otimes \begin{bmatrix} 0 \\ \mathbf{v} \end{bmatrix} \otimes \mathbf{q}^* = [\mathbf{q}^*]_R [\mathbf{q}]_L \begin{bmatrix} 0 \\ \mathbf{v} \end{bmatrix} = \begin{bmatrix} 0 \\ \mathbf{R}\mathbf{v} \end{bmatrix} \quad (\text{A.6})$$

From above the direct conversion from quaternion to rotation matrix can be obtained using (A.5) and results in:

$$\mathbf{R}\{\mathbf{q}\} = (q_w^2 - \mathbf{q}_v^T \mathbf{q}_v) \mathbf{I}_{3 \times 3} + 2\mathbf{q}_v \mathbf{q}_v^T + 2q_w [\mathbf{q}_v]_{\times} \quad (\text{A.7})$$

## A.1 Rotation vector to quaternion formula

The  $\mathbf{v} = \theta \mathbf{u}$  rotation vector represents rotation around  $\mathbf{u}$  axis with  $\theta$  angle. The operator is denoted by  $\mathbf{q}\{\mathbf{v}\}$  throughout this paper and can be written in the form of:

$$\mathbf{v} = \theta \mathbf{u} \Rightarrow \mathbf{u} = \frac{\mathbf{v}}{\|\mathbf{v}\|}, \quad \theta = \|\mathbf{v}\| \Rightarrow \mathbf{q}\{\mathbf{v}\} = \begin{bmatrix} \cos\left(\frac{\theta}{2}\right) \\ \sin\left(\frac{\theta}{2}\right) \mathbf{u} \end{bmatrix} = \begin{bmatrix} \cos\left(\frac{\|\mathbf{v}\|}{2}\right) \\ \sin\left(\frac{\|\mathbf{v}\|}{2}\right) \frac{\mathbf{v}}{\|\mathbf{v}\|} \end{bmatrix} \quad (\text{A.8})$$

## A.2 The time derivative of quaternion

When determining the time derivative of a vector, the goal is usually to specify the formula for the derivative in an inertial (fixed) frame with parameters known in a body (not fixed) frame which is only rotating, but not translating in the inertial frame.

Two approaches exist to writing the derivative of a quaternion: one is using an inertial frame-, other is using body frame- known parameters to describe the angular velocity. The angular velocity measurements are typically captured in the body frame, hence it is more practical to choose the second way.

Firstly, I will give the quaternion form of the angular velocity:

$$\begin{aligned}
\boldsymbol{\omega}_{\mathcal{L}}(t) &\triangleq \frac{d\boldsymbol{\phi}_{\mathcal{L}}(t)}{dt} = \lim_{\Delta t \rightarrow 0} \frac{\Delta\boldsymbol{\phi}_{\mathcal{L}}}{\Delta t} \stackrel{(A.8)}{=} \lim_{\Delta t \rightarrow 0} \frac{\mathbf{q}\{\Delta\boldsymbol{\phi}_{\mathcal{L}}\}}{\Delta t} = \lim_{\Delta t \rightarrow 0} \frac{\Delta\mathbf{q}_{\mathcal{L}}}{\Delta t} \\
&= \lim_{\Delta t \rightarrow 0} \frac{\begin{bmatrix} \cos(\Delta\theta_{\mathcal{L}}/2) \\ \sin(\Delta\theta_{\mathcal{L}}/2)\mathbf{u} \end{bmatrix}}{\Delta t} \approx \lim_{\Delta t \rightarrow 0} \frac{\begin{bmatrix} 1 \\ (\Delta\theta_{\mathcal{L}}/2)\mathbf{u} \end{bmatrix}}{\Delta t} = \lim_{\Delta t \rightarrow 0} \frac{\begin{bmatrix} 1 \\ \Delta\boldsymbol{\phi}_{\mathcal{L}}/2 \end{bmatrix}}{\Delta t} \quad (A.9)
\end{aligned}$$

Now, the next step is to write the time derivative of quaternion and use results from the previous equation:

$$\begin{aligned}
\frac{d\mathbf{q}(t)}{dt} &= \lim_{\Delta t \rightarrow 0} \frac{\mathbf{q}(t + \Delta t) - \mathbf{q}(t)}{\Delta t} = \lim_{\Delta t \rightarrow 0} \frac{\mathbf{q}_{\mathcal{L}} \otimes \mathbf{q} - \mathbf{q}}{\Delta t} \\
&= \lim_{\Delta t \rightarrow 0} \frac{(\mathbf{q}_{\mathcal{L}} - \mathbf{q}_1) \otimes \mathbf{q}}{\Delta t} = \lim_{\Delta t \rightarrow 0} \frac{\begin{bmatrix} 0 \\ \Delta\boldsymbol{\phi}_{\mathcal{L}}/2 \end{bmatrix} \otimes \mathbf{q}}{\Delta t} = \frac{1}{2} \begin{bmatrix} 0 \\ \boldsymbol{\omega}_{\mathcal{L}} \end{bmatrix} \otimes \mathbf{q}, \quad (A.10)
\end{aligned}$$

where the distributive property of quaternion product over sum was used, and  $\mathbf{q}_1$  denotes the identity quaternion<sup>1</sup>. It is crucial to note that, the  $\mathbf{q}(t + \delta t)$  quaternion is utilized by multiplying  $\mathbf{q}$  with  $\mathbf{q}_{\mathcal{L}}$  from left because it stands for Earth-to-body rotation.

---

<sup>1</sup> $\mathbf{q}_1 = [1 \ 0 \ 0 \ 0]^T$



### A.3 Jacobian of quaternion rotation with respect to the vector

To derive the derivative respected to the vector is very easy because the rotation matrix form can be applied:

$$\frac{\partial \mathbf{q} \otimes \mathbf{a} \otimes \mathbf{q}^*}{\partial \mathbf{a}} = \frac{\partial \begin{bmatrix} 0 \\ \mathbf{R}\mathbf{a} \end{bmatrix}}{\partial \mathbf{a}} = \mathbf{R} \quad (\text{A.11})$$

### A.4 Jacobian of quaternion rotation with respect to the quaternion

The derivative of the rotation with respect to the quaternion  $\mathbf{q}$  is a bit more difficult, but can be derived straightforwardly with the usage of (A.6) and (A.7).

Using a lighter notation for the quaternion:  $\mathbf{q} = \begin{bmatrix} w \\ \mathbf{v} \end{bmatrix}$ , the rotation is:

$$\mathbf{a}' = \mathbf{q} \otimes \mathbf{a} \otimes \mathbf{q}^* = \mathbf{R}\mathbf{a} = w^2\mathbf{a} - \mathbf{v}^T\mathbf{v}\mathbf{a} + 2\mathbf{v}\mathbf{v}^T\mathbf{a} - 2w \left[ \mathbf{a} \right]_{\times} \mathbf{v} \quad (\text{A.12})$$

The Jacobian by the quaternion can be achieved by calculating the derivative of the scalar- and vector- part:

$$\begin{aligned} \frac{\partial \mathbf{a}'}{\partial w} &= 2(w\mathbf{a} + \mathbf{v} \times \mathbf{a}) \\ \frac{\partial \mathbf{a}'}{\partial \mathbf{v}} &= 2(\mathbf{v}^T\mathbf{a}\mathbf{I}_3 + \mathbf{v}\mathbf{a}^T - \mathbf{a}\mathbf{v}^T - w \left[ \mathbf{a} \right]_{\times}) \end{aligned} \quad (\text{A.13})$$

Using these results the Jacobian with respect to quaternion is:

$$\frac{\partial (\mathbf{q} \otimes \mathbf{a} \otimes \mathbf{q}^*)}{\partial \mathbf{q}} = 2 \left[ w\mathbf{a} + \mathbf{v} \times \mathbf{a} \mid \mathbf{v}^T\mathbf{a}\mathbf{I}_3 + \mathbf{v}\mathbf{a}^T - \mathbf{a}\mathbf{v}^T - w \left[ \mathbf{a} \right]_{\times} \right] \quad (\text{A.14})$$

# APPENDIX B

## ESKF-RELATED EQUATIONS

---

All of the following formulas with little difference can be found in [18].

### B.1 True rotation matrix

Firstly, I would like to introduce the ODE of rotation matrices. The rotation matrices have orthogonal properties, therefore their inverse is equal to their transpose, which results in the:

$$\mathbf{R}\mathbf{R}^T = \mathbf{I} \quad (\text{B.1})$$

Considering the time derivative of the above yields:

$$\begin{aligned} \frac{d}{dt}(\mathbf{R}\mathbf{R}^T) &= \dot{\mathbf{R}}\mathbf{R}^T + \mathbf{R}\dot{\mathbf{R}}^T = 0 \\ \mathbf{R}\dot{\mathbf{R}}^T &= -\dot{\mathbf{R}}\mathbf{R}^T \quad /^T \\ \dot{\mathbf{R}}\mathbf{R}^T &= -(\dot{\mathbf{R}}\mathbf{R}^T)^T, \end{aligned} \quad (\text{B.2})$$

which means that,  $\dot{\mathbf{R}}\mathbf{R}^T$  is skew-symmetric matrix, therefore there exists an  $\omega$  vector which results in:

$$\begin{aligned} \dot{\mathbf{R}}\mathbf{R}^T &= \begin{bmatrix} \omega \end{bmatrix}_{\times} \quad / \leftarrow \cdot \mathbf{R} \\ \dot{\mathbf{R}} &= \begin{bmatrix} \omega \end{bmatrix}_{\times} \mathbf{R} \end{aligned} \quad (\text{B.3})$$

Here, the second row represents the ODE of rotation matrices, which creates a relationship between the derivative of a rotation function, denoted as  $r(t)$ , and a quantity represented by  $\omega$ . When considering the scenario around the origin, the certain equation simplifies to  $\dot{\mathbf{R}} = \begin{bmatrix} \omega \end{bmatrix}_{\times}$ . Here,  $\omega$  can be interpreted as the vector representing instantaneous angular velocities. This understanding sheds light on

the Lie algebra  $\text{so}(3)$ , which can be seen as the space of derivatives of  $r(t)$  at the origin. It also serves as the tangent space to  $\text{SO}(3)$ , the special orthogonal group describing three-dimensional rotations.

If  $\boldsymbol{\omega}$  is constant, (B.3) can be time integrated as:

$$\mathbf{R}(t) = e^{\left[\boldsymbol{\omega}t\right]_{\times}} \mathbf{R}(0) \quad (\text{B.4})$$

The  $e^{\left[\boldsymbol{\omega}t\right]_{\times}}$  expression stands for the rotation matrix related to  $\boldsymbol{\omega}t = \mathbf{v}$  rotation vector. This means that the error rotation vector  $\delta\boldsymbol{\theta}$  has the connection between the nominal- and the true- rotation matrix:

$$\mathbf{R}_t = \delta\mathbf{R}\mathbf{R} = e^{\left[\delta\boldsymbol{\theta}\right]_{\times}} \mathbf{R}, \quad (\text{B.5})$$

where the error rotation matrix is described as the exponential of the skew matrix of the error rotation vector, which can be written in Taylor series:

$$e^{\left[\delta\boldsymbol{\theta}\right]_{\times}} = \sum_{k=0}^{k \rightarrow \infty} \frac{1}{k!} \left[\delta\boldsymbol{\theta}\right]_{\times}^k \quad (\text{B.6})$$

After neglecting the second and higher order members we got the form in (3.4).

## B.2 Error-state equations

The error-state can be expressed easily as the composition of the true-state (3.5) and the nominal-state (3.8). As it was detailed in Chapter 3 the error state remains small therefore second-order errors are negligible.

### B.2.1 Position error

$$\begin{aligned} \delta\dot{\mathbf{p}}_n &= \dot{\mathbf{p}}_{n,t} - \dot{\mathbf{p}}_n = \mathbf{R}^T \left( \mathbf{I} - \left[\delta\boldsymbol{\theta}\right]_{\times} \right) (\mathbf{v}_b - \delta\mathbf{v}_b) - \mathbf{R}^T \mathbf{v}_b \\ &= -\mathbf{R}^T \left[\delta\boldsymbol{\theta}\right]_{\times} \mathbf{v}_b + \mathbf{R}^T \delta\mathbf{v}_b, \end{aligned} \quad (\text{B.7})$$

where nominal state and second-order error were simplified. Using the anti-commutative property of cross-product, it can be written in the form of:

$$\delta \dot{\mathbf{p}}_n = \mathbf{R}^T \delta \mathbf{v}_b + \mathbf{R}^T \left[ \mathbf{v}_b \right]_{\times} \delta \boldsymbol{\theta} \quad (\text{B.8})$$

## B.2.2 Angular error

Calculating the angular error equation requires more complicated steps because it desires to use the derivative rule of the quaternion product:

$$(\delta \dot{\mathbf{q}} \otimes \mathbf{q}) = \delta \dot{\mathbf{q}} \otimes \mathbf{q} + \delta \mathbf{q} \otimes \dot{\mathbf{q}} \quad (\text{B.9a})$$

$$= \delta \dot{\mathbf{q}} \otimes \mathbf{q} + \delta \mathbf{q} \otimes \frac{1}{2} \begin{bmatrix} 0 \\ \boldsymbol{\omega} \end{bmatrix} \otimes \mathbf{q} \quad (\text{B.9b})$$

In (B.9b) the definition of quaternion derivative was used for local angular velocities and earth-to-body rotation. This equation is equal to the dynamics of the true quaternion state, which is defined in (3.5b), therefore simplifying with the terminal  $\mathbf{q}$  and isolating  $\delta \dot{\mathbf{q}}$  yields:

$$\begin{aligned} 2\delta \dot{\mathbf{q}} &= \begin{bmatrix} 0 \\ \boldsymbol{\omega}_t \end{bmatrix} \otimes \delta \mathbf{q} - \delta \mathbf{q} \otimes \begin{bmatrix} 0 \\ \boldsymbol{\omega} \end{bmatrix} \\ &= \left( \left[ \mathbf{q} \right]_L \left\{ \begin{bmatrix} 0 \\ \boldsymbol{\omega}_t \end{bmatrix} \right\} - \left[ \mathbf{q} \right]_R \left\{ \begin{bmatrix} 0 \\ \boldsymbol{\omega} \end{bmatrix} \right\} \right) \delta \mathbf{q} \end{aligned} \quad (\text{B.10})$$

Converting  $\delta \dot{\mathbf{q}}$  to  $\delta \boldsymbol{\theta}$  and performing the matrix subtraction results in:

$$\begin{aligned} \begin{bmatrix} 0 \\ \delta \boldsymbol{\Theta} \end{bmatrix} &= \begin{bmatrix} 0 & -(\boldsymbol{\omega}_t - \boldsymbol{\omega})^T \\ \boldsymbol{\omega}_t - \boldsymbol{\omega} & \left[ \boldsymbol{\omega}_t + \boldsymbol{\omega} \right]_{\times} \end{bmatrix} \begin{bmatrix} 1 \\ \frac{\delta \boldsymbol{\Theta}}{2} \end{bmatrix} + O(\|\delta \boldsymbol{\Theta}\|^2) \\ &= \begin{bmatrix} 0 & -\delta \boldsymbol{\omega}^T \\ \delta \boldsymbol{\omega} & \left[ 2\boldsymbol{\omega} + \delta \boldsymbol{\omega} \right]_{\times} \end{bmatrix} \begin{bmatrix} 1 \\ \frac{\delta \boldsymbol{\Theta}}{2} \end{bmatrix} + O(\|\delta \boldsymbol{\Theta}\|^2) \end{aligned} \quad (\text{B.11})$$

From the above arises a scalar- and a vector- equality. The scalar part is formed by second-order infinitesimals, which is not very useful, therefore only the vector part should be expressed. After neglecting second-order terms and substituting parameters from Table 3.1 into the nominal- and error- parameters yields:

$$\delta\dot{\Theta} = \left[ \omega_m - \beta_\omega \right]_{\times} \delta\Theta - \delta\beta_\omega - \eta_\omega \quad (\text{B.12})$$

### B.2.3 Velocity error

The velocity error is derived very similarly to the position error:

$$\begin{aligned} \delta\dot{\mathbf{v}}_b = \dot{\mathbf{v}}_{b,t} - \dot{\mathbf{v}}_b = & \mathbf{a} + \delta\mathbf{a} + \left( \mathbf{I} + \left[ \delta\Theta \right]_{\times} \right) \mathbf{R}\mathbf{g} - \left[ \omega + \delta\omega \right]_{\times} (\mathbf{v}_b + \delta\mathbf{v}_b) \\ & - (\mathbf{a} + \mathbf{R}\mathbf{g} - \left[ \omega \right]_{\times} \mathbf{v}_b) \end{aligned} \quad (\text{B.13})$$

Simplifying with nominal state and neglecting second-order terms gives the following equation:

$$\delta\dot{\mathbf{v}}_b = \delta\mathbf{a} + \left[ \delta\Theta \right]_{\times} \mathbf{R}\mathbf{g} + \left[ \delta\omega \right]_{\times} \mathbf{v}_b - \left[ \omega \right]_{\times} \delta\mathbf{v}_b \quad (\text{B.14})$$

To achieve the final form of the equation, parameters inserted from Table 3.1 into the nominal- and error-state, which results in:

$$\begin{aligned} \delta\dot{\mathbf{v}}_b = & - \left[ \mathbf{R}\mathbf{g} \right]_{\times} \delta\Theta - \left[ \omega_m - \beta_\omega \right]_{\times} \delta\mathbf{v}_b - \delta\beta_a - \left[ \mathbf{v}_b \right]_{\times} \delta\beta_\omega \\ & - \eta_a - \left[ \mathbf{v}_b \right]_{\times} \eta_\omega \end{aligned} \quad (\text{B.15})$$

### B.3 Jacobian of true quaternion with respect to the error rotation vector

The relationship between the true quaternion and the error rotation vector can be determined using the chain rule, which can be formulated as follows:

$$\begin{aligned}
\frac{\partial(\delta\mathbf{q} \otimes \mathbf{q})}{\partial\delta\boldsymbol{\theta}} &= \frac{\partial(\delta\mathbf{q} \otimes \mathbf{q})}{\partial\delta\mathbf{q}} \frac{\partial\delta\mathbf{q}}{\partial\delta\boldsymbol{\theta}} \\
&= \frac{\partial\left(\left[\mathbf{q}\right]_R \delta\mathbf{q}\right)}{\partial\delta\mathbf{q}} \frac{\partial\begin{bmatrix} 1 \\ \frac{1}{2}\delta\boldsymbol{\theta} \end{bmatrix}}{\partial\delta\boldsymbol{\theta}} = \frac{1}{2} \left[\mathbf{q}\right]_R \begin{bmatrix} \mathbf{0}^T \\ \mathbf{I}_3 \end{bmatrix} \\
&= \frac{1}{2} \begin{bmatrix} -q_x & -q_y & -q_z \\ q_w & q_z & -q_y \\ -q_z & q_w & q_x \\ q_y & -q_x & q_w \end{bmatrix}
\end{aligned} \tag{B.16}$$

### B.4 Jacobian of reset function ( $\mathbf{g}$ ) with respect to the error rotation vector

The goal is to determine the derivative of (3.29b) by the error rotation vector  $\delta\boldsymbol{\theta}$ . Firstly, I aim to formalize that equation with rotation vector parameters, neglecting the constant terms:

$$\begin{aligned}
\mathbf{q}\{\delta\boldsymbol{\theta}\} \otimes \mathbf{q}\{-\hat{\delta}\boldsymbol{\theta}\} &= \left[\mathbf{q}\right]_R \left\{ \begin{bmatrix} 1 \\ -\frac{1}{2}\hat{\delta}\boldsymbol{\theta} \end{bmatrix} \right\} \begin{bmatrix} 1 \\ \frac{1}{2}\delta\boldsymbol{\theta} \end{bmatrix} + \mathcal{O}(\|\delta\boldsymbol{\theta}\|^2) \\
&= \begin{bmatrix} 1 & \frac{1}{2}\hat{\delta}\boldsymbol{\theta}^T \\ \frac{1}{2}\hat{\delta}\boldsymbol{\theta} & \mathbf{I} + \left[\frac{1}{2}\hat{\delta}\boldsymbol{\theta}\right]_{\times} \end{bmatrix} \begin{bmatrix} 1 \\ \frac{1}{2}\delta\boldsymbol{\theta} \end{bmatrix} + \mathcal{O}(\|\delta\boldsymbol{\theta}\|^2) \\
&= \begin{bmatrix} 1 + \frac{1}{4}\hat{\delta}\boldsymbol{\theta}^T \delta\boldsymbol{\theta} \\ \frac{1}{2}\hat{\delta}\boldsymbol{\theta} + \frac{1}{2} \left( \mathbf{I} + \left[\frac{1}{2}\hat{\delta}\boldsymbol{\theta}\right]_{\times} \right) \delta\boldsymbol{\theta} \end{bmatrix} + \mathcal{O}(\|\delta\boldsymbol{\theta}\|^2)
\end{aligned} \tag{B.17}$$

This is equal to the error quaternion after the reset. Denoting the error rotation vector with  $\delta\theta^+$  the following equation can be written:

$$\begin{bmatrix} 1 \\ \frac{1}{2}\delta\theta^+ \end{bmatrix} = \begin{bmatrix} 1 + \frac{1}{4}\hat{\delta\theta}^T \delta\theta \\ \frac{1}{2}\hat{\delta\theta} + \frac{1}{2} \left( \mathbf{I} + \left[ \frac{1}{2}\hat{\delta\theta} \right]_{\times} \right) \delta\theta \end{bmatrix} + \mathcal{O}(\|\delta\theta\|^2) \quad (\text{B.18})$$

The above equation splits into a scalar- and a vector- part, where the scalar part is formed by second-order infinitesimals, therefore it is not very useful, additionally the constant member in the original (3.29b) equation is responsible for exactly this neglect. Only considering the vector part, the Jacobian:

$$\frac{\partial g(\delta\theta)}{\partial \delta\theta} = \frac{\partial \delta\theta^+}{\partial \delta\theta} = \frac{\partial \left( \hat{\delta\theta} + \left( \mathbf{I} + \left[ \frac{1}{2}\hat{\delta\theta} \right]_{\times} \right) \delta\theta \right)}{\partial \delta\theta} = \mathbf{I} + \left[ \frac{1}{2}\hat{\delta\theta} \right]_{\times} \quad (\text{B.19})$$

# ABBREVIATIONS

---

BME	Budapesti Műszaki Egyetem
EKF	Extended Kalman Filter
ESKF	Error-State Kalman Filter
GPS	Global Positioning System
IMU	Inertial Measurement Unit
INS	Inertial Navigation System
KF	Kalman Filter
NED	North-East-Down
RMSE	Root Mean Square Error
SCL	System Control Laboratory
SZTAKI	Számítástechnikai és Automatizálási Kutatóintézet
UAS	Unmanned Aerial System
UAV	Unmanned Aerial Vehicle
3D	Three-dimensional



# LIST OF FIGURES

---

1.1	Block diagram of relative navigation ([7]: page 2, Figure 2) . . . . .	3
1.2	Realistic drawing of Cindy ([15]: title page) . . . . .	4
2.1	Applied coordinate systems . . . . .	5
2.2	Frames to define Euler angles ([10]: pages 13-15, Figures 2.4-2.7) . .	8
2.3	Camera and image system ([16]: page 7) . . . . .	10
4.1	Illustration of intersection (top) and resection (bottom) forms of the triangulation problem ([19]: page 3) . . . . .	28
6.1	Camera image example . . . . .	39
6.2	NED coordinates . . . . .	40
6.2	NED coordinates (Continued) . . . . .	41
6.3	Euler angles . . . . .	42
6.3	Euler angles (Continued) . . . . .	43
6.4	Body-fixed velocity . . . . .	43
6.4	Body-fixed velocity (Continued) . . . . .	44

# LIST OF TABLES

---

3.1	ESKF states and inputs . . . . .	16
6.1	Noise summary . . . . .	38

# BIBLIOGRAPHY

---

- [1] David Erdos, Abraham Erdos, and Steve E. Watkins. An experimental uav system for search and rescue challenge. *IEEE Aerospace and Electronic Systems Magazine*, 28(5):32–37, 2013.
  
- [2] Friedrich Fraundorfer, Lionel Heng, Dominik Honegger, Gim Hee Lee, Lorenz Meier, Petri Tanskanen, and Marc Pollefeys. Vision-based autonomous mapping and exploration using a quadrotor mav. In *2012 IEEE/RSJ International Conference on Intelligent Robots and Systems*, pages 4557–4564, 2012.
  
- [3] Abdulla Al-Kaff, Francisco Miguel Moreno, Luis Javier San José, Fernando García, David Martín, Arturo de la Escalera, Alberto Nieva, and José Luis Meana Garcéa. Vbii-uav: Vision-based infrastructure inspection-uav. In Álvaro Rocha, Ana Maria Correia, Hojjat Adeli, Luís Paulo Reis, and Sandra Costanzo, editors, *Recent Advances in Information Systems and Technologies*, pages 221–231, Cham, 2017. Springer International Publishing.
  
- [4] V. Tirronen H. Salo and F. Neri. Evolutionary regression machines for precision agriculture. In *Applications of Evolutionary Computation*, pages 356–365, Berlin, Heidelberg, 2012. Springer Berlin Heidelberg.
  
- [5] Stefan Leutenegger and Roland Y. Siegwart. A low-cost and fail-safe inertial navigation system for airplanes. In *2012 IEEE International Conference on Robotics and Automation*, pages 612–618, 2012.
  
- [6] Cesario Vincenzo Angelino, Vincenzo Rosario Baraniello, and Luca Cicala. High altitude uav navigation using imu, gps and camera. In *Proceedings of the 16th International Conference on Information Fusion*, pages 647–654, 2013.

- [7] Gary Ellingson, Kevin Brink, and Tim McLain. Relative navigation of fixed-wing aircraft in gps-denied environments. *NAVIGATION*, 67(2):255–273, 2020.
- [8] Sebastian Thrun, Wolfram Burgard, and Dieter Fox. *Probabilistic Robotics*. MIT Press, 2010.
- [9] David O. Wheeler, Daniel P. Koch, James S. Jackson, Timothy W. McLain, and Randal W. Beard. Relative navigation: A keyframe-based approach for observable gps-degraded navigation. *IEEE Control Systems Magazine*, 38(4):30–48, 2018.
- [10] RANDAL W. BEARD and TIMOTHY W. McLAIN. *Small Unmanned Aircraft: Theory and Practice*. Princeton University Press, 2012.
- [11] Stephan Weiss, Markus W. Achtelik, Simon Lynen, Margarita Chli, and Roland Siegwart. Real-time onboard visual-inertial state estimation and self-calibration of mavs in unknown environments. In *2012 IEEE International Conference on Robotics and Automation*, pages 957–964, 2012.
- [12] Timothy D. Barfoot and Paul T. Furgale. Associating uncertainty with three-dimensional poses for use in estimation problems. *IEEE Transactions on Robotics*, 30(3):679–693, 2014.
- [13] Robert C. Leishman, Timothy W. McLain, and Randal W. Beard. Relative navigation approach for vision-based aerial gps-denied navigation. *Journal of Intelligent & Robotic Systems*, 74(1–2):97–111, 2013.
- [14] David O. Wheeler, Paul W. Nyholm, Daniel P. Koch, Gary J. Ellingson, Timothy W. McLain, and Randal W. Beard. Relative navigation in gps-degraded environments. *Encyclopedia of Aerospace Engineering*, page 1–10, 2016.
- [15] István Gőzse, Máté Kisantal, Péter Onódi, and Pierre Arnaud. *Sindy UAV test platform assembly manual*. Institute for Computer Sciences and Control, 2016.
- [16] Kris Kitani. 8.2 camera matrix. Presentation slide, March 2017.

- [17] W. R. Hamilton. On a new species of imaginary quantities, connected with the theory of quaternions. *Proceedings of the Royal Irish Academy (1836-1869)*, 2:424–434, 1840.
- [18] Joan Solà. Quaternion kinematics for the error-state kalman filter. *CoRR*, abs/1711.02508, 2017.
- [19] Sébastien Henry and John A. Christian. Absolute triangulation algorithms for space exploration. *Journal of Guidance, Control, and Dynamics*, 46(1), 2022.
- [20] G. T. McCaw. Resection in survey. *The Geographical Journal*, 52(2):105–123, 1918.
- [21] Arun Bernard, Akhter Mahmud Nafi, and David Geller. Using triangulation in optical orbit determination. 09 2018.
- [22] Long Chen, Chengzhi Liu, Zhenwei Li, and Zhe Kang. A new triangulation algorithm for positioning space debris. *Remote Sensing*, 13(23), 2021.
- [23] Richard I. Hartley and Peter Sturm. Triangulation. *Comput. Vis. Image Underst.*, 68(2):146–157, nov 1997.
- [24] M Pollefeys, R Koch, M Vergauwen, and L Van Gool. Automated reconstruction of 3d scenes from sequences of images. *ISPRS Journal of Photogrammetry and Remote Sensing*, 55(4):251–267, 2000.
- [25] Noah Snavely, Steven M. Seitz, and Richard Szeliski. Modeling the world from internet photo collections. *Int. J. Comput. Vision*, 80:189–210, nov 2008.
- [26] James L. Poirot and Gerald V. McWilliams. Navigation by back triangulation. *IEEE Transactions on Aerospace and Electronic Systems*, AES-12(2):270–274, 1976.
- [27] Gene H. Golub and Charles F. Van Loan. *Matrix Computations - 4th Edition*. Johns Hopkins University Press, Philadelphia, PA, 2013.
- [28] Gabriel A. Terejanu. Discrete kalman filter tutorial.

- [29] D. S. Oliver. Gaussian cosimulation: Modelling of the cross-covariance. *Mathematical Geology*, 2003.
- [30] Szabolcs Kun. Image-based inertial navigation. Master's thesis, Budapest University of Technology and Economics, Budapest, Hungary, 5 2021.